J. Fluid Mech. (2002), *vol.* 473, *pp.* 349–377.
DOI: 10.1017/S0022112002002471 Printed in the United Kingdom

Liquid-fuel thermocapillary flow induced by a spreading flame

By F. J. HIGUERA

E. T. S. Ingenieros Aeronáuticos, Pza. Cardenal Cisneros 3, 28040 Madrid, Spain

(Received 8 March 2001 and in revised form 20 July 2002)

An analysis is presented of the flow in a layer of liquid whose surface tension varies under the action of a moving surface heat flux distribution chosen to model the spread of a flame over the liquid. Subject to this heat flux, the surface temperature increases from the ambient temperature of the liquid, far upstream, to its vaporization temperature at a moving vaporization front, and stays constant at this value downstream of the vaporization front. The speed of the front is determined by a condition of regularity of the temperature. Three different regimes are found which correspond to the uniform, pulsating and pseudo-uniform regimes of flame spread observed experimentally when the ambient temperature of the liquid, or the strength of the surface heat flux, is decreased. The first and third of these are stationary regimes of high and low front speed, and the second is an oscillatory regime featuring long phases of low speed and short pulses of high speed. An asymptotic description is given of the flow relative to the moving vaporization front in the stationary regime of low speed, which includes a long recirculation eddy ahead of the front and a small region around the front that controls its speed. An explanation of the mechanism of oscillation is proposed based on the interplay between the quasi-steady response of this small controlling region and the delay introduced by the recirculating flow.

1. Introduction

Flame spread over liquid fuels is a classic problem of combustion theory, which is of both fundamental interest and practical importance. At sufficiently high temperatures, vaporization of the fuel leads to a combustible fuel vapour–air mixture in a layer above the liquid surface. Upon ignition, a triple flame (Liñán 1994) may propagate in this layer without further heating or vaporization of the liquid. This mode of flame spread is fast and controlled by the gas phase – the only effect of the liquid being to quench the rich-side wing of the triple flame if it is too close to the surface – but it ceases to be possible when the liquid temperature and its vapour pressure decrease. Then, below a certain critical temperature dependent on the fuel, flame spread requires that part of the heat released by the flame in the gas phase be used to heat and vaporize the liquid, so as to create a combustible mixture locally. This brings in mechanisms of heat and mass transfer in both phases that make the spread slower than in the high-temperature mode. One such mechanism, first pointed out by Sirignano & Glassman (1970; see also references therein), is heat convection in the liquid phase by the thermocapillary and buoyancy flows induced by the variation of surface tension and density from the high-temperature region below the flame to the ambient temperature ahead of the flame. Typically surface tension is a decreasing function of temperature and thermocapillary stresses tend to pull the liquid away

from the flame, in the direction of propagation, preheating this upstream region and enhancing flame spread. The buoyancy-generated pressure force acts in the same direction but is somewhat less important than thermocapillary stresses in many cases. Both mechanisms are specific to liquid fuels, as opposed to solid fuels, and seem to be responsible for some of the observed differences between the two types of fuel.

Experiments with narrow open channels filled with alcohols or hydrocarbons have been carried out by Mackinver, Hansel & Glassman (1968), Akita (1973), Ito, Masuda & Saito (1991), Miller & Ross (1995), Degroote & García-Ybarra (2000), and Miller *et al.* (2000), among others; see Ross (1994) and Ross & Miller (1997) for reviews. These experiments, along with numerical simulations (Furuta, Humphrey & Fernández-Pello 1985; Di Blasi, Crescitelli & Russo 1990, 1991; Schiller, Ross & Sirignano 1996; Schiller & Sirignano 1997; Kim, Schiller & Sirignano 1999), reveal three different spread regimes for liquid temperatures below the critical value mentioned above. These are a stationary regime in a temperature range immediately below the critical value, an oscillatory regime in an intermediate temperature range, and a second stationary regime at still lower temperatures. Akita (1973) named these regimes uniform, pulsating and pseudo-uniform, respectively. The first regime is not unlike flame spread over solid fuels, and there is some debate about the presence and importance of thermocapillarity-induced recirculation ahead of the flame in this regime (Hirano *et al.* 1980; Glassman & Dryer 1981; Ito *et al.* 1991; Schiller *et al.* 1996; Degroote & García-Ybarra 2002). Thermocapillary stresses are clearly important in the pulsating regime, which has no analogue for solid fuels. As the temperature of the liquid is decreased in the range of this regime, the spread rate oscillates with increasing amplitude and decreasing frequency, and the oscillations feature long phases of slow spread (crawling phases), during which a large recirculation region of warm liquid forms ahead of the flame, and short phases of fast spread (jump phases), during which the flame front advances over the preheated liquid. The period of the oscillations diverges at a certain value of the liquid temperature, below which the spread again becomes stationary but with a much reduced rate and a long recirculation region preceding the flame. The name given by Akita to this third regime points to the difficulty of realizing it neatly in channels of finite length.

Much work has been devoted to trying to understand the mechanisms that control flame spread in the different regimes, the transitions between them and, in particular, the causes of pulsating spread. A number of different proposals have been developed. Akita & Fujiwara (1971) and Akita (1973) emphasized the role of the liquid flow around the surface and ahead of the flame, pointing out the strong differences shown by this region in the uniform and pulsating regimes, and suggesting that the presence of reverse flow upstream of the flame promotes unsteady spreading, except in the pseudo-uniform regime. Glassman & Dryer (1981) favoured the view of a coupling or periodic switching between gas-phase conduction and liquid-phase convection control in the pulsating regime, with the combustion alternating between a fast premixed burning stage and a slow diffusive burning stage during which fuel vapour accumulates in front of the flame. This view has been adopted and developed by many authors, including Di Blasi *et al.* (1990), Ito *et al.* (1991) and Miller & Ross (1998); see also the extensive review of Ross (1994).

Schiller *et al.* (1996) and Schiller & Sirignano (1997) carried out two-dimensional numerical computations for the pulsating and uniform regimes using a detailed physical model that includes liquid- and gas-phase buoyancy and unsteadiness, thermocapillary stresses at the interface, and a finite-rate one-step gas-phase chemical reaction. These authors link pulsating spread to the presence of a gas-phase recir-

culation cell ahead of the flame and attribute a critical role in the flame pulsation cycle to the gas expansion near the reaction zone. The gas cell forms during the phase of crawling spread due to the combination of the flow induced in the gas by thermocapillary stresses, which is concurrent with flame propagation, and the opposing flow due to buoyancy or to an opposing forced stream. The cell grows and accumulates fuel vapour until, at a certain moment, the flame accelerates through the premixed region thus formed. The associated surge of hot gas expansion destroys the cell during the jump phase of the pulsation. Then the flame slows after consuming the available fuel vapour and waits for the cell to regenerate. Schiller *et al.* (1996) and Schiller & Sirignano (1997) discuss the influence on the nature of flame spread of the initial liquid temperature and depth, oxygen concentration in the ambient gas, opposed air velocity, and fuel volatility, among other factors, by looking at their effects on the gas-phase recirculation cell. Their findings are in qualitative agreement with experiments. For both the pulsating and the uniform regime, these authors conclude that combustion occurs in a mixed mode at the flame leading edge, with a lean premixed region ahead of the flame and combustion of excess air with fuel vapour that diffuses from below the reaction zone, and also that liquid-phase convection driven by thermocapillarity is the dominant mechanism of heat transfer ahead of the flame. Realizing that channel sidewalls and lateral hot gas expansion might be limiting the accuracy of two-dimensional simulations, Kim *et al.* (1999) extended the work of Schiller and coworkers to axisymmetric spread over shallow circular pools, where these effects are not present, and obtained good quantitative agreement with experiment.

Buckmaster & Zhang (1999) and Buckmaster, Hegab & Jackson (2000) proposed a different mechanism of oscillation dependent solely on the gas phase. These authors suggest that the pulsating regime of flame spread is one of a number of manifestations of oscillating edge flames, which are brought about by the combination of a well-known high Lewis number instability (Williams 1985) and the reduced-strength burning conditions prevailing at the edge of a flame sheet. They note a number of cases where their general principle might apply, ranging from the combustion of condensed fuels to candle flames in microgravity, and examine simple conceptual models of anchored flames where oscillations and other responses can be realized by changing the Lewis number of the fuel, a Damköhler number, and some other parameters. The proposal has sound physical bases and is appealing in its universality. Further work should ascertain its validity in each particular instance.

For the motion of the liquid, Sirignano & Glassman (1970) evaluated thermocapillary convection as a rate-controlling mechanism in a layer of viscosity-dominated flow. Sharma & Sirignano (1971) extended this analysis to cases where viscous forces are confined to a surface boundary layer much thinner than the liquid layer, and García-Ybarra *et al.* (1996) found that the flow is self-similar around the upstream end of the boundary layer. Torrance (1971) and Torrance & Mahajan (1975*a*,*b*) studied the thermocapillary flow induced by a heat source moving at a constant speed over a quiescent liquid and raising the surface temperature under the source to a constant value. By solving numerically the Navier–Stokes and energy equations for the liquid, these authors obtained qualitative pictures of the velocity and temperature fields and investigated the influence of the Reynolds number, the Prandtl number, the speed of the source and the Grashof number, when buoyancy is taken into account. Further numerical results and an asymptotic analysis of this model problem for large Reynolds numbers were presented in Higuera & García-Ybarra (1998), who also found oscillations resembling those of the pulsating regime in conditions such that

the only effect of the gas is to supply a time-independent heat flux, with assigned distribution and strength, to the liquid surface upstream of the vaporization front. Evidently, the origin of these oscillations is to be sought in the dynamics of the liquid.

The purpose of this work is to study the thermocapillary flow induced in the liquid by the spreading of a flame over its surface, in order to ascertain the role of the liquid-phase in the different regimes of flame spread. To this end, a simplified model will be adopted that permits the dynamics of the liquid around the advancing vaporization front to be isolated from the complex processes going on in the gas. If the liquid is assumed to vaporize at a constant temperature, which is an admissible approximation for liquids of simple molecular structure, and the vaporization flux crossing the surface is neglected in the region around the vaporization front, then the only influence of the gas on the liquid in this region comes through the heat flux reaching the surface. This heat originates at the nose of the flame in the gas and should be determined by an analysis of the gas flow, which depends on such complicating factors as the vaporization flux, the level of body forces, the possible presence of a forced stream, and the reaction kinetics, among others. All this results in a formidable problem, but a kind of minimal model can be formulated by lumping all the gas-affecting factors into a model distribution of the heat flux that reaches the liquid. This approach has been used in other combustion problems and was employed in Higuera & García-Ybarra (1998). The only free parameters of the model are the width and strength of the surface heat flux distribution, which will be taken to be constant, while the distribution itself moves with the unknown speed of the vaporization front. These parameters have clear physical meanings and their effect will be studied along with that of the parameters characterizing the liquid, but it should be stressed that they are parameters of the model, not primitive variables. A limitation of this procedure is that it ignores the pulsations of the shape and strength of the heat flux distribution that accompany the pulsating spread of real flames. The simplified model is not intended to simulate the spread of any real flame, but it is still useful to investigate the contribution of the liquid phase to the overall process.

The minimal problem is formulated in § 2. The results for stationary spread are presented in § 3, while § 4 is devoted to a qualitative analysis of the structure of the flow for large Reynolds numbers, giving special attention to a small region around the vaporization front that controls the spread rate. The results for oscillatory spread are presented in § 5, and finally § 6 is a summary of the conclusions.

2. Formulation

Consider a horizontal layer of liquid fuel which is heated and vaporized by a travelling heat source intended to model the front of a flame spreading over the liquid surface. The liquid vaporizes at its surface when the surface temperature reaches a constant temperature T_v higher than the initial temperature of the liquid T_0. Neglecting the effect of any possible recondensation, all the heat reaching the non-vaporizing region of the surface, where the temperature is smaller than T_v, enters the liquid. In the vaporizing region of the surface, on the other hand, the temperature is equal to T_v and only a part of the heat enters the liquid, the rest being used to vaporize it. The heat flux reaching the surface around the vaporization front (where the surface temperature first reaches the value T_v) is modelled as a constant distribution moving with the front. The effect of the vaporization mass flux on the dynamics of the liquid around the vaporization front is neglected in comparison with the larger fluxes prevailing in the bulk of the liquid (see below). This model makes the dynamics of the liquid independent of the gas, except for the global features of

the latter that are reflected in the surface heat flux distribution. In particular, any oscillatory or complex response of the system should be ascribed to the liquid.

For a pure liquid, the constant-vaporization-temperature model, with T_v equal to the boiling temperature of the liquid at the pressure of the gas above it, follows from the thermodynamic phase-equilibrium condition in the asymptotic limit $L\mathscr{M}/RT_v \to \infty$, where L and $\mathscr{M}$ are the heat of vaporization per unit mass and the molecular mass of the liquid, and R is the universal gas constant (see e.g. Liñán 1985). Thus the Clapeyron–Clausius equilibrium law

$$Y = \frac{\mathscr{M}}{\mathscr{M}_g} \exp\left[\frac{\beta(\theta-1)}{1+(1-T_0/T_v)(\theta-1)}\right],$$

where Y is the mass fraction of fuel vapour at the surface, $\mathscr{M}_g$ is the mean molecular mass of the gas, $\beta = (L\mathscr{M}/RT_v)(T_v - T_0)/T_v$, and $\theta = (T - T_0)/(T_v - T_0)$, restricts appreciable vaporization [$Y = O(1)$] to the range $(1-\theta) = O(\beta^{-1})$. The parameter β is often moderately large, and the constant-vaporization-temperature model is widely used. The transition from non-vaporizing to vaporizing surface occurs in the narrow region, idealized as a front, where the surface temperature first enters this range. With a proper choice of T_v, the constant-vaporization-temperature model is also useful to represent irreversible rate evaporation processes with high activation energy (which takes the place of L in β above); see Wichman (1992). When none of this is applicable, appreciable vaporization occurs at ambient temperature, and the vapour content of the gas depends on geometrical and other details of the system and on its previous history, making it difficult to obtain general results.

The effects of the buoyancy and the deformation of the surface are neglected. Estimates presented elsewhere (Higuera & García-Ybarra 1998) show that buoyancy may have a marginal effect in some cases but is not the main cause of the liquid motion in the conditions of most flame spread experiments. This role is played by thermocapillary stresses, due to the variation of the surface tension in the region of the surface where the temperature increases from T_0 to T_v. These stresses push the liquid toward the cool region ahead of the flame and will be taken here as the only cause of the motion of the liquid relative to the bottom of the channel.

In a reference frame moving with the vaporization front, with the vaporizing surface extending to $x > 0$, the flow of the liquid, assumed to be two-dimensional, is governed by the following equations:

$$\nabla \cdot \boldsymbol{v} = 0, \tag{2.1}$$

$$Re\left(\frac{\partial \boldsymbol{v}}{\partial t} + \boldsymbol{v}\cdot\nabla\boldsymbol{v}\right) = -\nabla p + \nabla^2 \boldsymbol{v}, \tag{2.2}$$

$$Re\,Pr\left(\frac{\partial \theta}{\partial t} + \boldsymbol{v}\cdot\nabla\theta\right) = \nabla^2\theta; \tag{2.3}$$

$$y = 0: \begin{cases} v = 0, \quad \dfrac{\partial u}{\partial y} + \dfrac{\partial \theta}{\partial x} = 0, \\ \dfrac{\partial \theta}{\partial y} = q_g(x) \text{ for } x < 0 \quad \text{and} \quad \theta = 1 \text{ for } x > 0; \end{cases} \tag{2.4a,b,c}$$

$$y = -1: \quad u = U, \quad v = \theta = 0; \tag{2.5}$$

$$x \to -\infty: \quad u = U, \quad v = \theta = 0, \quad \frac{\partial p}{\partial x} = -Re\frac{\mathrm{d}U}{\mathrm{d}t}; \tag{2.6}$$

$$x \to \infty: \quad u = U, \quad v = 0, \quad \theta = 1 + y. \tag{2.7}$$

Here x and y are distances along and normal to the surface scaled with the depth of the layer h, the liquid occupying the strip $-1 \leqslant y \leqslant 0$; $\theta = (T - T_0)/(T_v - T_0)$ is the reduced temperature introduced above; $\boldsymbol{v} = (u, v)$ is the velocity of the liquid relative to the vaporization front and U is the spread rate, or velocity of the front relative to the bottom of the channel, all of them scaled with $v_c = |\sigma'|(T_v - T_0)/\mu$, where $\sigma' = \mathrm{d}\sigma/\mathrm{d}T < 0$ is taken to be a constant; t is the time scaled with h/v_c; and p is a modified pressure scaled with $|\sigma'|(T_v - T_0)/h$. The two non-dimensional parameters entering (2.2) and (2.3) are a Reynolds number and the Prandtl number of the liquid,

$$Re = \frac{\rho|\sigma'|(T_v - T_0)h}{\mu^2} \quad \text{and} \quad Pr = \frac{c\mu}{k}, \tag{2.8}$$

where ρ, μ, k and c are the liquid density, viscosity, thermal conductivity and specific heat.

The non-dimensional modified pressure in (2.2) and (2.6) is

$$p = \widetilde{p} + Gy - Re\frac{\mathrm{d}U}{\mathrm{d}t}x,$$

where $\widetilde{p}$ is the static pressure of the liquid scaled with $|\sigma'|(T_v - T_0)/h$ and $G = \rho g h^2/|\sigma'|(T_v - T_0)$, with g the acceleration due to gravity. The third term in the definition of the modified pressure is the potential of the fictitious body force that appears because the reference frame moving with the front is not inertial when $\mathrm{d}U/\mathrm{d}t \neq 0$. Far from the front, the thermocapillary stress is zero and the liquid is at rest relative to the bottom of the layer, so that $\boldsymbol{v} = (U, 0)$ in the moving frame, as is stated in (2.6) and (2.7). The horizontal component of the left-hand side of (2.2) reduces to $Re\,\mathrm{d}U/\mathrm{d}t$ in this far region, and this horizontal acceleration is balanced by the negative of the horizontal gradient of the modified pressure. This is the last condition (2.6). The uniform gradient of the modified pressure far from the front is due to the third term in the definition of p, while the static pressure $\widetilde{p}$ is bounded.

No balance of stresses normal to the surface of the liquid is included in the formulation (2.1)–(2.7). This balance could be used to determine the small deformation of the surface after problem (2.1)–(2.7) (where the deformation is neglected) has been solved.

The boundary condition (2.4b) at the surface ($y = 0$) is the balance of thermocapillary and viscous stresses. The boundary condition (2.4c) is specific to the constant-vaporization-temperature model. The heat flux reaching the surface, $q_g(x)$, is prescribed in the non-vaporizing region $x < 0$, while $\theta = 1$ in the vaporizing region $x > 0$. The heat flux entering the liquid through the vaporizing surface is determined by the solution of the problem. This heat flux is not equal to the heat flux reaching the surface (the extension of $q_g(x)$ to $x > 0$); the difference is used to vaporize the liquid. The heat flux $q_g(x)$, which is scaled with $k(T_v - T_0)/h$, is a key element of the problem. It will be modelled by a Gaussian distribution

$$q_g(x) = q_0 \exp\left(-\frac{x^2}{\lambda^2}\right) \quad \text{for} \quad x < 0, \tag{2.9}$$

where the strength q_0 measures the exothermicity of the gas-phase reactions and will be used as a control parameter in what follows. Since q_0 is scaled with $k(T_v - T_0)/h$, it increases with the ambient temperature T_0 for a given fuel and oxygen concentration in the gas. This is a convenient connection because T_0 is the control parameter most commonly used in experimental work.

Problem (2.1)–(2.7) describes the thermocapillary flow induced in a layer of liquid by a travelling heat source. The heat source moves with velocity U above the liquid, supplies the surface with the heat flux distribution (2.9) for $x < 0$, and leaves a vaporizing surface for $x > 0$ (modelled here by the condition $\theta = 1$ after Torrance 1971 and Torrance & Mahajan 1975*a*, *b*). The problem should have a solution for any assigned $U(t)$. However, not all these solutions are appropriate to represent the flow induced by a spreading flame. This is because, in general, the heat flux that needs to enter the liquid to achieve the condition $\theta = 1$ for $x \geqslant 0$ turns out to diverge strongly when the vaporization front is approached from behind ($x \searrow 0$), while a real flame in the gas cannot supply such a diverging heat flux. Thus, even though the heat flux reaching the vaporizing surface does not appear explicitly in the formulation (2.1)–(2.7), the condition that this flux, having the same origin as $q_g(x)$ in (2.9), is limited and cannot diverge arbitrarily for $x \searrow 0$ will determine the spread rate.

To find the form of the divergence of the heat flux and the condition selecting U so as to mimic a spreading flame, consider the vicinity of the vaporization front $x = y = 0$. In the present constant-vaporization-temperature model, this is a singular point around which heat conduction, responsible for the highest-order derivatives in (2.3), dominates. With the boundary condition (2.4*c*), the temperature is locally the harmonic function $\theta = 1 + A\, r^{1/2} \sin \varphi/2$ for any $q_g(x)$ less singular than $(-x)^{-1/2}$ ahead of the origin, for which, effectively, $q_g = 0$ at leading order (when compared with $|\nabla\theta| = O(r^{-1/2})$ around the origin); see Higuera (1999) for details. Here $r = \sqrt{x^2 + y^2}$ and $\varphi = \arctan y/x$ are polar coordinates and A is a constant that cannot be determined by a local analysis but comes from matching with the solution further away from the origin, and thus depends on U, Re, Pr, the whole distribution of $q_g(x)$, and time (in non-stationary cases).

This local form of the temperature has often been found before; see e.g. Fernández-Pello, Kindelán & Williams (1974) , Wichman & Williams (1983) and Wichman (1992). Here it is not admissible because the square-root singularity requires a surface heat flux diverging as $A/(2\,x^{1/2})$ at the right of the origin, to keep $\theta = 1$ there, which cannot be supplied by the gas. Consistency requires therefore that $A = 0$, and since A depends on U and the parameters of the problem, this condition of minimal singularity determines U as a function of these parameters, and of the time in cases of non-stationary spreading. A related problem in which a more localized heat source supplying a Gaussian heat flux distribution to the surface travels with an assigned speed U along the surface is discussed in the Appendix. Vaporization occurs then in a finite region whose boundaries are to be determined to avoid square-root singularities.

Further analysis of the temperature around the origin, once the square-root singularity is ruled out, has been carried out in Higuera (1999) assuming that the energy is released in the gas phase by a diffusion flame with infinitely fast kinetics. This analysis shows that $\theta - 1 = O(r \log r)$ and the surface heat flux diverges only logarithmically at the vaporization front, a divergence that is taken care of by the gas phase. In other cases, the logarithmic singularity may be smoothed out in the narrow region of transition from non-vaporizing to vaporizing surface, inducing logarithmic terms in an asymptotic expansion for $\beta^{-1} \to 0$. Guided by these results, a model $q_g(x)$ with a logarithmic singularity at the origin has been used in some simulations, multiplying (2.9) by a factor $f(x/\lambda)$, where $f(\xi) = \log[(\xi - a)/\xi]/\log[(\epsilon + a)/\epsilon]$, with a and ϵ constant, the second equal to the pitch of the finite difference grid at the origin (see below). The results obtained with this alternative heat flux distribution show that the logarithmic singularity is not important to the overall flow.

The width and strength of the heat flux distribution (2.9) can be related to the conditions of the gas around the front of the spreading flame. The dimensional width of the Gaussian, λh, measures the size of the gas region around the flame front where upstream heat conduction is important. Leaving aside conditions of massive aiding flow (a strong gas flow in the direction of flame spreading), which probably would require a separate analysis, the characteristic size of this region is α_g/v_g (Liñán 1994), where α_g is the thermal diffusivity of the gas and v_g is its characteristic local velocity. This latter quantity may take a wide range of values, depending on whether the gas flow is due to opposing forced convection, natural convection, or the drag of the liquid. The characteristic temperature elevation of the gas around the flame is $\Delta T_g = (Q/c_p)/(1+s)$ (Williams 1985), where Q is the heat released by the combustion of a unit mass of fuel, c_p is the specific heat of the gas at constant pressure, and s is the air-to-fuel mass stoichiometric ratio, or mass of air needed to burn the unit mass of fuel. The heat flux in the region of the gas around the flame front is therefore of order $k_g \Delta T_g/\lambda$, where k_g is the thermal conductivity of the gas. This should be the order of q_0 in dimensional variables.

The total energy released per unit time by the flame in this region is of order $k_g \Delta T_g = (k_g/c_p)Q/(1+s)$. This energy is to be compared with the flux of chemical energy associated with the flow rate of liquid fuel relative to the flame, equal to ρUhQ. The ratio $(k_g \Delta T_g)/(\rho UhQ)$ is of order $\epsilon_1 = (\mu_g/\mu)/[(1+s)Re]$, where μ_g is the viscosity of the gas and a factor $Pr_g = \mu_g/(k_g/c_p)$, which is of order unity, has been left out. This ratio is small because the gas-to-liquid viscosity ratio is small and the Reynolds number and s are large ($s \approx 10.4$ for propanol in air). Thus only a small fraction of the chemical energy of the fuel is consumed around the flame front. The rest of the liquid flows pass this region, being vaporized and burned only further downstream, if at all. The rate at which the fuel is consumed downstream of the flame front depends on the conditions of the gas flow (forced convection, natural convection, microgravity, etc), but a flame is typically left downstream of the vaporization front that is amply able to keep the liquid vaporizing. A lower bound estimate of the distance it would take to deplete the chemical energy in the liquid layer can be obtained by assuming that the heat flux released by the flame is of the order of q_0 in this far region, which is a gross overestimation. Then the distance to full depletion of the liquid layer would be of order λ/ϵ_1. This distance is taken here to be sufficiently large that the downstream conditions (2.7), and the condition that the depth of the liquid is equal to its value upstream of the front, still hold in a large intermediate region.

The vaporization flux at the right of the origin, which was neglected in the formulation, can now be estimated. Since a fraction of the heat flux reaching the surface for $x > 0$, which is of the same order q_0 as for $x < 0$, is used to vaporize the liquid, the mass flux across the vaporizing surface is $\rho v = O(q_0/L)$ in dimensional variables, where L is the heat of vaporization. In non-dimensional variables, this amounts to a term of order $q_0[c(T_v - T_0)/L]/(Re\,Pr)$ on the right-hand side of the boundary condition (2.4*a*). This is a small term because $c(T_v - T_0)/L$ is moderately small, of the order of 0.1–0.2 for the first aliphatic alcohols in typical experimental conditions, and the product $Re\,Pr$ is large. Insofar as the vaporization rate is small compared with the spread rate, most of the liquid that flows under the advancing front is vaporized and consumed by the flame only very far downstream of the front, in line with the estimates of the previous paragraph. If the vaporization rate were of order q_0/L everywhere on the vaporizing surface, the order of the distance it would take to deplete the liquid layer would coincide with the distance estimated in the previous paragraph up to a factor of order L/Q.

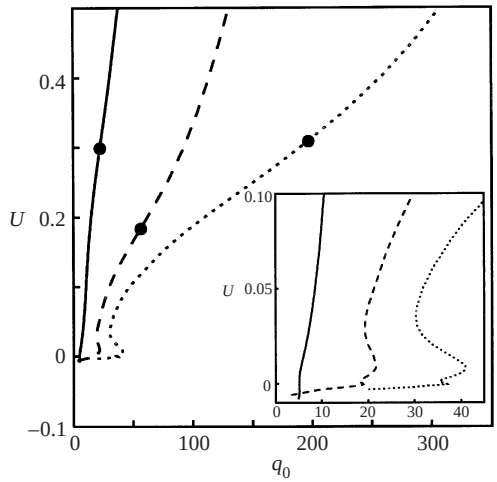

FIGURE 1. Stationary spread rate as a function of q_0 for $Pr = 10$ and $(Re, \lambda) = (100, 0.2)$ (solid), (1000, 0.2) (dashed), and (1000, 0.02) (dotted). The solid circles mark the beginning of recirculation.

Problem (2.1)–(2.7), with $q_g(x)$ given by (2.9) and the regularity condition at the origin discussed above, has been solved numerically using the vorticity–stream function formulation for (2.1) and (2.2) and second-order finite differences. This formulation removes the modified pressure from the problem. Non-stationary solutions for a given q_0 have been computed by a standard coupled transient method, second order in time, with implicit discretization of the diffusion terms and biconjugate gradient iteration. Stationary solutions were computed most easily by means of a pseudo-transient method in which a constant value is assigned to U and q_0 is determined iteratively.

3. Stationary spreading

The stationary spread rate is shown in figure 1 as a function of q_0 for $Pr = 10$ and different values of Re and λ. While $Pr = 10$ is typical of some liquid fuels, and numerical results for somewhat higher Prandtl numbers are similar to those of figure 1, the values of Re used in the present computations are smaller than in typical experiments by a factor of 10 to 100. This restriction to low Reynolds numbers is necessary to keep the computations affordable in view of the complex structure of the solution in the asymptotic limit $Re \to \infty$, to be discussed in the following section. The results, however, display the qualitative features documented experimentally.

The spread rate U increases quadratically with q_0 for large values of this parameter in the three cases shown in figure 1. This is because the effect of the thermocapillary stresses is negligible at high spread rates and the liquid moves with nearly uniform velocity relative to the vaporization front, as if it were a solid. The surface flux heats the liquid in a thin thermal layer ahead of the vaporization front where the energy equation reduces to $Re\,Pr\,U\,\partial\theta/\partial x = \partial^2\theta/\partial y^2$ with the boundary conditions $\partial\theta/\partial y = q_g(x)$ at $y = 0$ and $\theta = 0$ for $x \to -\infty$ and for $y \to -\infty$ (in the liquid flowing under the thermal layer). From the solution of this problem, $\theta(0,0) = 2\int_{-\infty}^{0}(-x)^{1/2}(\mathrm{d}q_g/\mathrm{d}x)\,\mathrm{d}x/(\pi\,Re\,Pr)^{1/2} = (\Gamma(1/4)/2\pi^{1/2})(\lambda/Re\,Pr\,U)^{1/2}q_0$, and the condition that $\theta = 1$ at the vaporization front determines the spread rate

$$U = \frac{\Gamma^2(1/4)}{4\pi}\frac{\lambda q_0^2}{Re\,Pr} \approx 1.0461\frac{\lambda q_0^2}{Re\,Pr}, \tag{3.1}$$

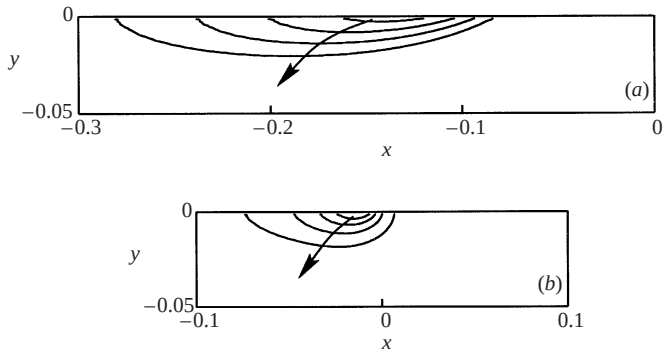

FIGURE 2. Recirculation bubble for $Re = 1000$ and $Pr = 10$ in four cases with incipient recirculation. In (a), for $\lambda = 0.2$, the spread rates of the cases displayed are $U = 0.18, 0.17, 0.16$ and 0.15, decreasing in the direction of the arrow. In (b), for $\lambda = 0.02$, $U = 0.28, 0.25, 0.22$ and 0.19, decreasing in the direction of the arrow.

which in dimensional terms amounts to a spread rate proportional to the depth h of the liquid and inversely proportional to $(T_v - T_0)^2$, in qualitative agreement with experimental results (Miller & Ross 1992).

The characteristic thickness of the thermal layer is $\lambda^{1/2}/(Re\,Pr\,U)^{1/2} \sim 1/q_0$, from the balance of longitudinal convection and transverse conduction in the energy equation. Similarly, the thickness of the viscous layer where thermocapillary stresses affect the velocity is $\delta_v = \lambda^{1/2}/(Re\,U)^{1/2} \sim Pr^{1/2}/q_0$. The velocity variation across this layer is of order $\Delta u = \delta_v/\lambda$, from (2.4$b$). This variation becomes of the order of U, invalidating (3.1), when $q_0 = O(Re^{1/3}Pr^{1/2}/\lambda^{2/3})$, provided $\delta_v/\lambda = O[(\lambda Re)^{-1/3}]$ is still small, in order for the boundary layer approximation to be applicable. In any case, a critical value of q_0 exists, marked by a solid circle on each curve of figure 1, below which there is a recirculation region ahead of the vaporization front. The size of this region increases with decreasing q_0 and its presence very rapidly affects the heat transfer around the origin, where the regularity condition must be satisfied.

The dividing streamline bounding the recirculation region for some values of q_0 slightly below the critical value is plotted in figure 2 for $Re = 1000$, $Pr = 10$ and the two values $\lambda = 0.2$ and $\lambda = 0.02$ corresponding to the dashed and dotted curves of figure 1, respectively. As can be seen, recirculation first appears at a distance upstream of the vaporization front that increases with λ, the width of the surface heat flux distribution. This result will have a bearing on a type of oscillations to be discussed in § 5.

The two curves for $Re = 1000$ in figure 1 present a range of multiplicity and a lower branch for small spread rates, revealing a mode of propagation essentially different from the high-velocity solid-like mode discussed above. The range of multiplicity does not exist for $Re = 100$, for which case the presence of recirculation merely changes the curvature of the response curve. It should be noted that multiplicity could be just a feature of the constant-q_0 model. The state of the gas phase above the liquid should be different in the different solutions for a given q_0, and thus different values of this parameter would have been obtained if q_0 had been evaluated from an analysis of the gas phase instead of being assigned. In all the cases q_0 has a positive value when $U = 0$, increases slightly with decreasing U in a very narrow range around $U = 0$, and then decreases again when U becomes more negative.

Some streamlines and isotherms for $Re = 5000$, $Pr = 10$, $\lambda = 0.2$ and different

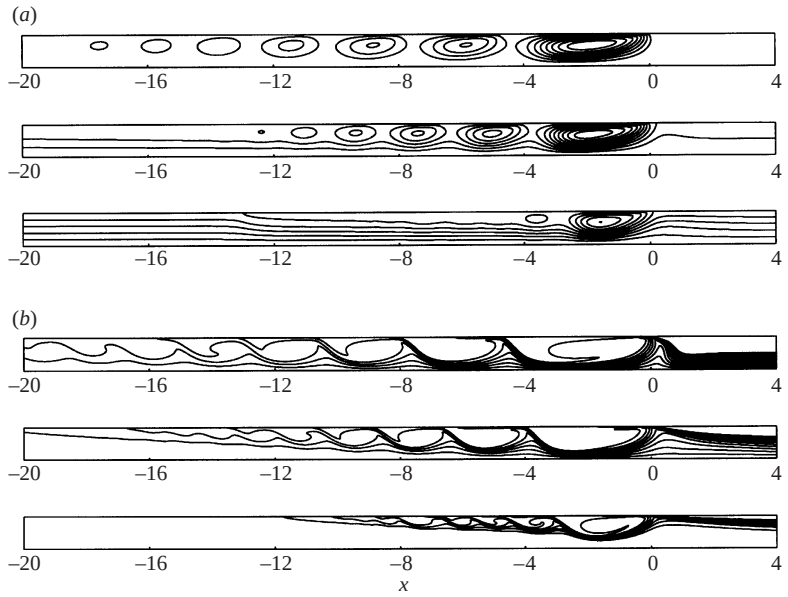

FIGURE 3. (*a*) Streamlines and (*b*) isotherms for $Re = 5000$, $Pr = 10$, $\lambda = 0.2$ and three values of the spread rate; $U = 0$, 0.001 and 0.005, increasing from top to bottom. Displayed in each case are eight streamlines between 5×10^{-4} and 4×10^{-3}, ten streamlines between -5×10^{-4} and 4×10^{-3}, and eleven streamlines between -5×10^{-3} and 5×10^{-3}, respectively, and eleven isotherms between $\theta = 0$ and $\theta = 0.5$, in the three cases.

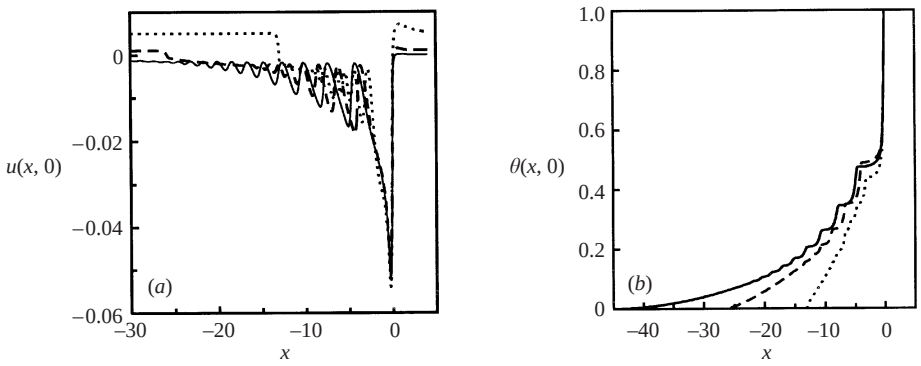

FIGURE 4. (*a*) Surface velocity and (*b*) surface temperature for the cases of figure 3. $U = 0$ (solid), 0.01 (dashed), and 0.05 (dotted).

values of the spread rate in the lower branch of the response curve are given in figure 3. The surface velocity and temperature are given in figure 4. As can be seen, there is a main eddy immediately ahead of the vaporization front followed by other, weaker eddies if the spread rate is sufficiently small, and by an elongated surface tongue further to the left. The recirculation region extends much further upstream of the vaporization front than downstream of it, and its length decreases with increasing U. The temperature field shows a richer structure than the velocity field because the Prandtl number is large. In all the cases the temperature drops steeply at the left of the front, tends to be uniform in the eddies, and decreases smoothly to the ambient temperature at a finite distance from the front. Global balances of momentum and

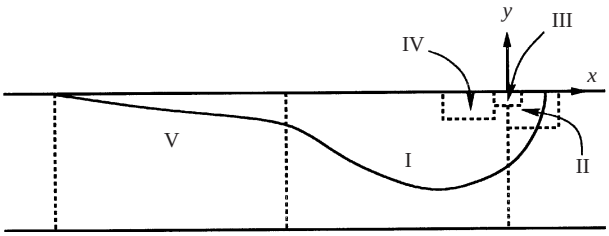

FIGURE 5. Sketch of the regions of the stationary flow for $Re \gg 1$ and small spread rates. Not to scale.

forces evaluated with the numerical solutions show that the flow in the eddies is due to the thermocapillary force imparted to the liquid in the region of steep surface temperature drop, which appears as a point source of momentum for the bulk of this flow, and that the recirculating flow at the left of the eddies is driven by local thermocapillary stresses.

4. Asymptotic estimations for low spread rates

The asymptotic form of the low-speed stationary solutions for large values of Re and moderately large Pr is of some interest. The asymptotic structure of the flow is sketched in figure 5. This flow is characterized by a very long recirculation bubble and is realized only in the pseudo-uniform regime, because the actual solution is oscillatory in part of the range covered by the asymptotic orders-of-magnitude description that follows. Despite this limitation, some elements of the description, especially those concerning the region around the vaporization front, will be useful to understand the mechanics of the oscillatory solutions in § 5.

4.1. *Bulk of the recirculation bubble*

The total force imparted to the liquid by the strong thermocapillary stresses immediately to the left of the vaporization front is $-\int (\partial u/\partial y)_{y=0} \mathrm{d}x = \int (\partial\theta/\partial x)\,\mathrm{d}x = O(1)$, from (2.4*b*), where the integrals extend to the region of steep temperature drop. To the left of this region, this force induces a surface jet of thickness and characteristic velocity $\delta_j = (-x)^{2/3}/Re^{1/3}$ and $u_j = Re^{-1/3}(-x)^{-1/3}$, respectively. These estimates come from the order-of-magnitude balance of longitudinal convection and transverse diffusion in the momentum equation (2.2), $Re\, u_j^2/(-x) = u_j/\delta_j^2$, and the condition $Re\, u_j^2\delta_j = 1$, expressing that the momentum flux of the jet is of the order of the applied force.

Left to itself, the jet would open and cover the whole liquid layer ($\delta_j = O(1)$) at a distance of order $x_1 = Re^{1/2}$ to the left of the origin (region I of figure 5), where the velocity is of order $u_1 = Re^{-1/2}$. Friction with the bottom in this region gives rise to an overpressure that prevents the extension of the recirculating flow further away from the origin. The x_1 and u_1 above are the characteristic length and velocity of the recirculating flow when the spread rate U is of order u_1 or smaller. They are compared with the numerical results in figure 6(*a*), where the abscissa of the centre of the main eddy and the maximum value of the stream function, which is a measure of the velocity of the recirculating flow, are plotted as functions of Re for the solutions with $U = 0$. The agreement with the asymptotic power laws is good even at the moderate values of Re of these computations. The comparison also shows that the size of the eddy is numerically small compared with $Re^{1/2}$; note the coefficient 0.03

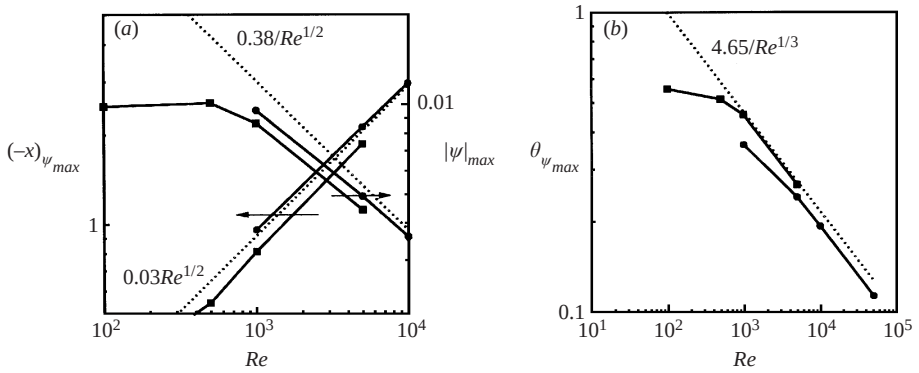

FIGURE 6. (*a*) Horizontal distance from the centre of the main eddy to the vaporization front (left ordinate) and stream function at the centre (right ordinate), and (*b*) temperature at the centre, as functions of the Reynolds number for $U = 0$, $\lambda = 0.2$ and $Pr = 1$ (circles) and $Pr = 10$ (squares). The dotted lines have the slopes predicted by the asymptotic analysis.

obtained by fitting the $Re^{1/2}$ law to the numerical results. The characteristic length of the recirculation region decreases to $x_1' = Re^{-1}U^{-3}$ when $U \gg u_1$ (from the condition $u_j(x_1') \sim U$).

4.2. *Recirculation region at the right of the origin*

Expanded views of the recirculation region at the right of the origin in the cases in figure 3 (not shown) suggest that the flow around the rear end of the eddy, at $x = x_2$ say, is affected by the local entrainment of the jet. The entrainment induces velocities of order $u_e = u_j\delta_j/|x| = Re^{-2/3}|x|^{-2/3}$ at distances from the origin of the order of the depth of the liquid layer, $|x| = O(1)$, or smaller. The condition $u_e(x_2) = O(U)$ gives $x_2 = O(Re^{-1}U^{-3/2})$, which makes sense if $U = O(Re^{-2/3})$ or larger, so that $x_2 = O(1)$ or smaller. The length x_2 should be of $O(1)$ for still smaller values of U, which would have little effect on the local flow. Thus, summarizing, the characteristic length and velocity of the recirculating flow in region II at the right of the origin are

$$x_2 = O\left[\min\left(\frac{1}{Re\,U^{3/2}}, 1\right)\right] \quad \text{and} \quad u_2 = O\left[\max\left(U, \frac{1}{Re^{2/3}}\right)\right]. \tag{4.1}$$

Having determined these scales, it is now possible to estimate the heat flux entering the liquid that recirculates under the warm vaporizing surface between the rear end of the eddy ($x = x_2$) and the origin. The temperature of this liquid changes from $\theta = 0$ to $\theta = 1$ across a surface thermal layer of characteristic thickness $\delta_{2_T} = (x_2/Re\,Pr\,u_2)^{1/2}$, obtained from the balance of longitudinal convection and transverse conduction in (2.3). Therefore $\partial\theta/\partial y = O(1/\delta_{2_T})$ and the total heat flux received by the liquid is $Q_2 = \int_0^{x_2} (\partial\theta/\partial y)_{y=0}\,\mathrm{d}x = O(x_2/\delta_{2_T}) = O(Re\,Pr\,x_2)^{1/2}$.

Denoting $u_s(x) = u(x, 0) < 0$ the surface velocity, and introducing the new variable $\xi = \int_0^x u_s\,\mathrm{d}x = O(u_2x_2)$ and the stream function $\psi \approx yu_s$, of order $\psi_{2_T} = (u_2x_2/Re\,Pr)^{1/2}$ in the thermal layer, the energy equation reduces to $Re\,Pr\,\partial\theta/\partial\xi = \partial^2\theta/\partial\psi^2$ in this layer, to be solved with the boundary conditions $\theta = 1$ at $\psi = 0$, $\theta = 0$ for $\psi/\psi_{2_T} \to \infty$, and appropriate conditions at the rear end of the eddy, where $\xi = \int_0^{x_2} u_2\mathrm{d}x$, or at infinity if $U \ll Re^{-2/3}$. The solution of this problem would give, in particular, a smooth temperature distribution $\theta = \theta_0(\psi/\psi_{2_T})$ at $\xi = 0$, though $\partial\theta/\partial y = u_s\partial\theta/\partial\psi$ diverges at the origin because the entrainment of the surface jet to the left of the origin dominates the flow locally and leads to a diverging u_s.

4.3. *Navier–Stokes region around the origin*

This singularity is resolved in a smaller region III around the origin where viscous forces and thermocapillary stresses (for $x < 0$) come into play. The subscript *ns*, standing for Navier–Stokes, will be used to denote the characteristic scales of this region, to emphasize that it is not slender and the full Navier–Stokes equations have to be solved in it. Thus x_{ns} and u_{ns} will denote the characteristic length and velocity of region III, and $\Delta\theta_{ns}$ the characteristic temperature variation (about $\theta = 1$) in the subregion where heat conduction is important. This can be the whole region III, if $Pr = O(1)$, or a layer of thickness $\delta_{ns_T} = x_{ns}/Pr^{1/2}$, if the Prandtl number is large. The balances of convection and viscous forces in the momentum equation (2.2) and of thermocapillary and viscous stresses at the surface yield the order of magnitude relations $Re\, u_{ns}^2/x_{ns} = u_{ns}/x_{ns}^2$ and $\Delta\theta/x_{ns} = u_{ns}/x_{ns}$. A third relation, closing the problem, can be obtained by noticing that the mass flux in the heat conduction layer, of order $\phi_{ns_T} = u_{ns}x_{ns}/Pr^{1/2}$, comes from the uppermost part of the thermal layer in region II, where $\theta = \theta_0(\psi/\psi_{2_T}) \approx 1 - B(\psi/\psi_{2_T})$ with $B = -\theta_0'(0) = O(1)$. Thus $\Delta\theta_{ns} = B\,\phi_{ns_T}/\psi_{2_T}$, where the constant B is retained for convenience. From this and the two previous relations,

$$x_{ns} = \frac{Pr^{1/2}\psi_{2_T}}{B} = \frac{(u_2x_2)^{1/2}}{B\,Re^{1/2}}, \quad u_{ns} = \Delta\theta_{ns} = \frac{B}{Re\,Pr^{1/2}\psi_{2_T}} = \frac{B}{(Re\,u_2x_2)^{1/2}}, \tag{4.2}$$

with $u_2x_2 = \min(Re^{-1}U^{-1/2}, Re^{-2/3})$ from (4.1).

Equations (2.1)–(2.4) do not change form when the variables are rescaled with these factors (the rescaled variables are denoted with capital letters in what follows) and $\Theta = (\theta - 1)/\Delta\theta_{ns}$ is used instead of θ, except that Re disappears from (2.2) and (2.3), and (2.4*c*) becomes $\partial\Theta/\partial Y = \tilde{q}_0$ for $X < 0$ and $\Theta = 0$ for $X > 0$, where $\tilde{q}_0 = q_0\,x_{ns}/\Delta\theta_{ns}$ (because $q_0(x) \approx q_0$ in the present small region).

These equations must be complemented with far-field boundary conditions. Far from the origin viscous forces and heat conduction become negligible except in a thermocapillary-driven surface jet to the left of the origin. The liquid outside this jet conserves its temperature on each streamline, equal to $\Theta = -Pr^{1/2}\Psi$ in rescaled variables, insofar as it comes from the upper part of the thermal layer of region II. Asymptotically, for $(-X) \gg 1$, the stream function and the temperature in the jet take the form $\Psi = (-X)^{1/2}f(\eta)$ and $\Theta = (-X)^{1/2}g(\eta)$, with $\eta = Y/(-X)^{1/2} = O(1)$ and

$$\left.\begin{gathered} 2f''' - ff'' = 0, \\ 2g'' + Pr(f'g - fg') = 0, \\ \eta = 0 : f = 0, \quad f'' - \tfrac{1}{2}g = 0, \quad g' = \tilde{q}_0, \\ \eta \to -\infty : f' = 0, \quad g = -Pr^{1/2}f. \end{gathered}\right\} \tag{4.3}$$

The solution of this problem determines, in particular, $f_\infty = \lim_{\eta\to-\infty} f$ as a function of Pr and $\tilde{q}_0$.

The flow in the rest of the far field is induced by the entrainment of the surface jet and has the stream function

$$\Psi = -f_\infty R^{1/2} \sin\frac{\varphi}{2}$$

in rescaled polar coordinates.

The description of the surface jet can be simplified for large values of Pr. Then the effect of heat conduction is confined to a sublayer where $\eta_T = Pr^{1/2}\eta = O(1)$ and $f \approx f_0'\eta$, with $f_0' = f'(0)$. The equation for g reduces to $2g'' + f_0'(g - \eta_T g') = 0$,

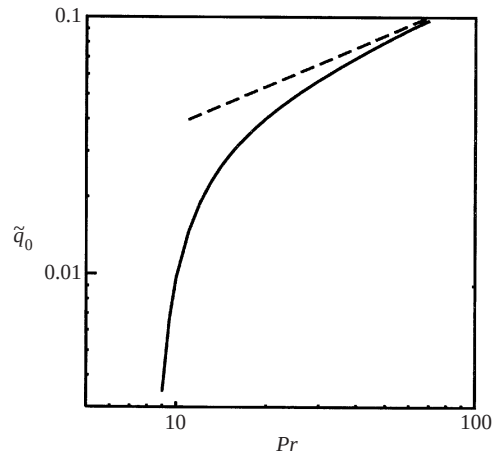

FIGURE 7. Rescaled heat flux strength, $\tilde{q}_0$, as a function of the Prandtl number, from the numerical solution of the Navier–Stokes equations in region III.

where primes denote now derivatives with respect to η_T, with the boundary conditions $g'(0) = \tilde{\tilde{q}}_0 = \tilde{q}_0/Pr^{1/2}$ and $g \to f_0'\eta_T$ for $\eta_T \to -\infty$. Its solution is

$$g = g(0)\left\{\exp\left(\frac{f_0'\eta_T^2}{4}\right) + \frac{\pi^{1/2}}{2}(-f_0')^{1/2}\eta_T \operatorname{erfc}\left(-\frac{(-f_0')^{1/2}}{2}\eta_T\right)\right\} + f_0'\eta_T,$$

with

$$g(0) = \frac{2}{\pi^{1/2}}(-f_0')^{1/2}\left(1 + \frac{\tilde{\tilde{q}}_0}{f_0'}\right).$$

Putting this $g(0)$ into the surface boundary condition for f in (4.3) leads to a problem containing only the parameter $\tilde{\tilde{q}}_0$ whose solution yields f_∞ as a function of this parameter.

This completes the specification of the far-field boundary conditions for region III. The solution of the problem should satisfy the same regularity condition at the origin as discussed in § 2 for the whole problem. This condition now determines a $\tilde{q}_0(Pr)$, which has been computed numerically and is given in figure 7. From these numerical results, $\tilde{q}_0 = \tilde{\tilde{q}}_0 Pr^{1/2}$, with $\tilde{\tilde{q}}_0 \approx 0.012$, for $Pr \gg 1$. Coming back to the original variables, the asymptotic relation between q_0 and U in the lower branch of the response curve can be written as

$$q_0 = B^2\tilde{\tilde{q}}_0 Pr^{1/2} Re^{2/3} \max(Re^{1/3}U^{1/2}, 1), \tag{4.4}$$

where $B = O(1)$ should be determined from the solution of the surface thermal layer in region II and depends on whether $U \gg Re^{-2/3}$, in which case the origin of this layer is at the rear end of the eddy $x = x_2$ estimated before, or $U \ll Re^{-2/3}$, in which case the thermal layer comes from far downstream of the origin. The result (4.4) for $U \gg Re^{-2/3}$ shows the same square-root dependence of q_0 on U as (3.1) for large values of q_0 in the upper branch of the response curve. The structure of the flow, however, is very different in the two cases. Notice, finally, that while (3.1) is clearly displayed by the dashed and dotted curves of figure 1, the lower branch of these curves is too short, for the moderate Reynolds numbers used in the computations, for (4.4) to be well resolved.

The form in which the results (4.2) and (4.4) are written depends on the particular estimate of $\Delta\theta_{ns}$ used in the paragraph above (4.2). This estimate came from an order-of-magnitude analysis of the surface thermal layer in region II to the right of the origin, but the small Navier–Stokes region III may also exist in cases when the analysis of the surface thermal layer is not applicable, as for example in the oscillatory solutions of the following section. All that matters, as far as the Navier–Stokes region is concerned, is the characteristic temperature difference between streamlines entering this region from behind and ending up in its thermal layer. This can be rewritten as $\Delta_{ns}\theta = (\mathrm{d}\theta/\mathrm{d}\psi)\phi_{ns_T}$, where the first factor, which takes the place of B/ψ_{2_T} used previously, depends on the conditions of the flow coming from the right and the second factor is always $u_{ns}x_{ns}/Pr^{1/2}$. Using this form of $\Delta\theta_{ns}$, (4.2) and (4.4) become

$$x_{ns} = \frac{Pr^{1/2}}{\mathrm{d}\theta/\mathrm{d}\psi}, \quad u_{ns} = \Delta\theta_{ns} = \frac{\mathrm{d}\theta/\mathrm{d}\psi}{Re\,Pr^{1/2}}, \quad q_0 = \frac{\tilde{\tilde{q}}_0}{Re\,Pr^{1/2}}\left(\frac{\mathrm{d}\theta}{\mathrm{d}\psi}\right)^2.$$

The third condition, in particular, means that $\mathrm{d}\theta/\mathrm{d}\psi$ in the liquid entering the Navier–Stokes region from behind has to be a constant determined by the values of the parameters q_0, Re and Pr and independent of the state of the rest of the flow. When this condition ceases to be satisfied the solution of the Navier–Stokes region ceases to satisfy the condition of regularity at the origin and the whole flow must undergo an abrupt transition.

Thus, in the lower branch of figure 1 the flow adjusts to an increase of q_0 by increasing U, so that the rear end of the recirculation bubble moves toward the origin, the thickness of the surface thermal layer decreases, and $\mathrm{d}\theta/\mathrm{d}\psi$ increases. This, however, also decreases the length of the recirculation region when u becomes of order $u_1 = Re^{-1/2}$, and then the recirculating liquid in the lower part of the eddy has less time to lose heat (see below), so that it may enter the surface thermal layer with $\theta > 0$, which tends to decrease $\mathrm{d}\theta/\mathrm{d}\psi$. The lower branch ends when this effect offsets that of decreasing the thickness of the surface thermal layer.

4.4. *Thermal effects to the left of the origin*

The characteristic thickness of the self-similar surface jet described by (4.3) continues to increase as $\delta_j = x_{ns}^{1/2}(-x)^{1/2}$ (in the original variables), and the characteristic velocity and heat flux in the jet remain equal to u_{ns} and q_0, while the thermal sublayer of the jet, of thickness $\delta_{j_T} = \delta_j/Pr^{1/2}$, continues to entrain warm liquid from the thermal layer of region II. This regime comes to an end when $\phi_{j_T} = u_{ns}\delta_{j_T}$ becomes of the order of ψ_{2_T}, estimated previously; i.e. at distances of order $x_4 = (u_2x_2)^{3/2}Re^{1/2} = Re^{-1/2}\min(Re^{-1/2}U^{-3/4}, 1) \ll x_2$ to the left of the origin, which is the characteristic length of the steep surface temperature drop (region IV of figure 5). The ratio of the total heat given to the liquid to the left of the origin, $\int_{-\infty}^{0} q_g\,\mathrm{d}x = \pi^{1/2}\lambda q_0/2$, to the characteristic heat Q_2 entering the recirculating liquid from the vaporizing surface to the right of the origin is of order λ/x_4. If λ is of order x_4 or smaller, then the surface jet takes the self-similar Bickley's form used previously to estimate x_2 when $(-x) \gg x_4$. If $\lambda \gg x_4$, then the jet becomes self-similar only for $(-x) \gg \lambda$, and the surface temperature to the left of the origin would first decrease and then increase beyond x_4, a feature observed in some experiments (Ross 1994; Konishi *et al.* 2000). The estimates above show that Q_2 decreases and q_0 increases with increasing U, so that this condition should be obtained for sufficiently high spread rates. In the computations shown in figure 3 the lower branch ends before this condition can be realized.

The recirculating liquid loses heat through the lower boundary of the eddy, either to the cool liquid flowing underneath or directly to the bottom. When $U \ll u_1 = Re^{-1/2}$, the incoming liquid occupies a thin layer under the eddy, of characteristic thickness $\delta \ll 1$ say, where the velocity is of order $u = u_1\delta$ (because of the non-slip condition at the bottom). The mass conservation balance $u_1\delta^2 = O(U)$ gives $\delta = U^{1/2}Re^{1/4}$. The thickness of the thermal layer around the dividing streamline bounding the eddy is $\delta_T = Re^{-1/8}Pr^{-1/2}U^{-1/4}$, from the convection–conduction balance $Re\,Pr\,(u_1\delta)/x_1 = 1/\delta_T^2$ with $x_1 = Re^{1/2}$. If $\delta_T \ll \delta$, which amounts to $U \gg Re^{-1/2}Pr^{-2/3}$, then heat is lost by the non-recirculating liquid at a rate $\int_{eddy}(\partial\theta/\partial y)\,\mathrm{d}x = O(x_1\theta_1/\delta_T) = Re^{5/8}Pr^{1/2}U^{1/4}\theta_1$, where θ_1 is the characteristic temperature of the recirculating liquid, to be determined. If this condition is not satisfied, then heat is lost by conduction to the bottom, in a thermal layer of thickness $\delta_T = 1/Pr^{1/3}$ (the convection–conduction balance is $Re\,Pr\,(u_1\delta_T)/x_1 = 1/\delta_T^2$ in this case), at a rate of order $x_1\theta_1/\delta_T = Re^{1/2}Pr^{1/3}\theta_1$. In summary, the recirculating liquid loses heat at a rate $Re^{1/2}Pr^{1/3}\theta_1 \max(Re^{1/8}Pr^{1/6}U^{1/4}, 1)$. In order to determine θ_1, this quantity must be equated to the total heat given to the liquid per unit time $Q_2 + \pi^{1/2}\lambda q_0/2$. Assuming, for definiteness, that the second term of this sum is not much larger than the first, and using the estimate of Q_2 worked out before, this heat balance gives

$$\theta_1 = \frac{Pr^{1/6}}{Re^{1/3}}\frac{\min(1/Re^{1/6}U^{1/4}, 1)}{\max(Re^{1/8}Pr^{1/6}U^{1/4}, 1)}.$$

The presence of the min and max functions in this expression leads to a number of different regions in the (Re, Pr, U) space. The result, however, can be summarized approximately as

$$\theta_1 = \frac{Pr^{1/6}}{Re^{1/3}} \quad \text{if} \quad U \ll Re^{-2/3}\min(1, (Re/Pr^4)^{1/6}), \tag{4.5a}$$

$$\theta_1 = \frac{1}{U^{1/2}Re^{5/8}} \quad \text{if} \quad U \gg Re^{-2/3}\max(1, (Re/Pr^4)^{1/6}), \tag{4.5b}$$

because typically $(Re/Pr^4)^{1/6}$ is not very different from unity and the intermediate range where none of these estimates apply is small. The estimate (4.5*a*) is compared with the numerical solution of (2.1)–(2.7) in figure 6(*b*). Notice finally that the estimate of the heat loss must be modified when U is large compared with u_1, to take into account the reduced length of the eddy. The previous balance changes then to $\theta_1 = U^{3/4}$.

4.5. *Heat transfer at the left of the eddy for* $Pr \gg 1$

The temperature excess of the recirculating liquid above the ambient temperature leads to thermocapillary stresses far to the left of the origin which, when $Pr \gg 1$, originate the elongated surface tongues apparent in figure 3. Two possibilities exist for the structure of the flow in this region V of figure 5. It can be a viscosity-dominated flow with heat convection balancing conduction across the whole layer, in which case the characteristic length and velocity are $x_5 = (Re\,Pr\,\theta_1)^{1/2}$ and $u_5 = (\theta_1/Re\,Pr)^{1/2}$, obtained from the convection–conduction balance $Re\,Pr\,u_5/x_5 = 1$ and the balance of viscous and thermocapillary stresses at the surface $u_5 = \theta_1/x_5$. These estimates hold insofar as $u_5 \gg U$. If this condition is violated, then the incoming flow impedes the development of a viscosity-dominated region V and the local thermocapillary

stresses lead to a viscous boundary layer under the surface, of characteristic length $x_5 = \theta_1^2/Re\,U^3$ and thickness $\delta_5 = \theta_1/Re\,U^2$ (from the balances of convection and viscous forces in (2.2), $Re\,U/x_5 = 1/\delta_5^2$, and of viscous and thermocapillary stresses $U/\delta_5 = \theta_1/x_5$), with heat conduction confined to a sublayer of thickness $\delta_5/Pr^{1/3}$ where the velocity is of order $U/Pr^{1/3}$. These estimates hold if $\delta_5 \ll 1$. Using the previous results for θ_1, it can be seen that the viscosity-dominated and boundary layer regimes correspond roughly to the ranges of (4.5*a*) and (4.5*b*), respectively. Under conditions leading to a boundary layer, the heat lost by the liquid recirculating in region V is always small compared with the heat lost by the bulk of the eddy (region I). In the viscosity-dominated regime, on the other hand, this condition may be violated if $Pr \gg Re^{2/3}$, in which case most of the heat given to the recirculating liquid is lost in region V and the estimates of θ_1 above become invalid.

The boundary layer regime has been analysed by García-Ybarra *et al.* (1996), showing that the temperature varies initially as the square root of the distance to the upstream end of the boundary layer. In the viscosity-dominated regime the momentum equation reduces to $0 = -\mathrm{d}p/\mathrm{d}x + \partial^2 u/\partial y^2$, with the conditions $u = U$ at $y = -1$, $\partial u/\partial y + \partial\theta/\partial x = 0$ at $y = 0$, and $\int_{-1}^{0} u\,\mathrm{d}y = U$. The solution of this problem determines u in terms of $(\partial\theta/\partial x)_{y=0}$, and the continuity equation then gives v. Using these results, the energy equation takes the form

$$Re\,Pr\left\{\left[-\frac{1}{4}\left(\frac{\partial\theta}{\partial x}\right)_{y=0}(1+y)(1+3y)+U\right]\frac{\partial\theta}{\partial x}+\frac{1}{4}\left(\frac{\partial^2\theta}{\partial x^2}\right)_{y=0}y(1+y)^2\frac{\partial\theta}{\partial y}\right\}=\frac{\partial^2\theta}{\partial y^2},$$

with $\theta = 0$ at $y = -1$ and for $x \to -\infty$, and $\partial\theta/\partial y = 0$ at $y = 0$. In addition, a condition of matching with the bulk of the eddy is required, of the form $\theta = \theta_{1s}$ in the leftward moving liquid entering the viscosity-dominated region, where $\theta_{1s} = O(\theta_1)$ is the surface temperature at the end of region I. The horizontal extent of the viscosity-dominated region V is finite, of the order of x_5, and the solution near its upstream end, at $x = x_e$ say, depends on whether $U = 0$ or $U > 0$. In the first case, which has been studied elsewhere (Higuera 2000), the temperature is locally of the form $\theta = (x - x_e)^2\Theta_1(y)$. When $U > 0$ the temperature around x_e is $\theta = 0$ except in a thin surface layer where $\eta = y/(x - x_e)^{1/3} = O(1)$ and the solution is of the form $\theta = (x - x_e)\Theta_1(\eta) + (x - x_e)^{4/3}\Theta_2(\eta) + \cdots$. Putting this expansion into the energy equation and collecting terms of orders 1 and $(x - x_e)^{1/3}$ leads to $\Theta_1(0) = 4U$ and $-Re\,Pr\,\left(4U\eta - \frac{1}{4}\Theta_2(0)\right)\left(\Theta_1 - \frac{1}{3}\eta\Theta_1'\right) = \Theta_1''$, with $\Theta_1'(0) = \Theta_1(\infty) = 0$. The latter problem has a solution only if $\Theta_2(0)(Re\,Pr)^{1/3}/2^{10/3}U^{2/3} \approx 1.0635$.

The linear and quadratic dependences of the surface temperature on $x - x_e$ for $U > 0$ and $U = 0$, respectively, are clearly displayed by the numerical results of figure 4(*b*).

5. Oscillatory spreading

Numerical solutions, computed by means of a fully transient method with q_0 constant and U evaluated at each time step to satisfy the condition of regularity at the origin, become time periodic, after an initial transient, in a certain range of values of q_0. Some properties of these periodic solutions, which correspond to the pulsating regime, are summarized in figure 8 for $Re = 1000$, $Pr = 10$ and two different values of λ. Plotted in this figure are the minimum and maximum spread rate U during the oscillation cycle, as functions of q_0, as well as the stationary spread rate discussed in the previous sections. Also plotted is the period of the oscillation P, while the

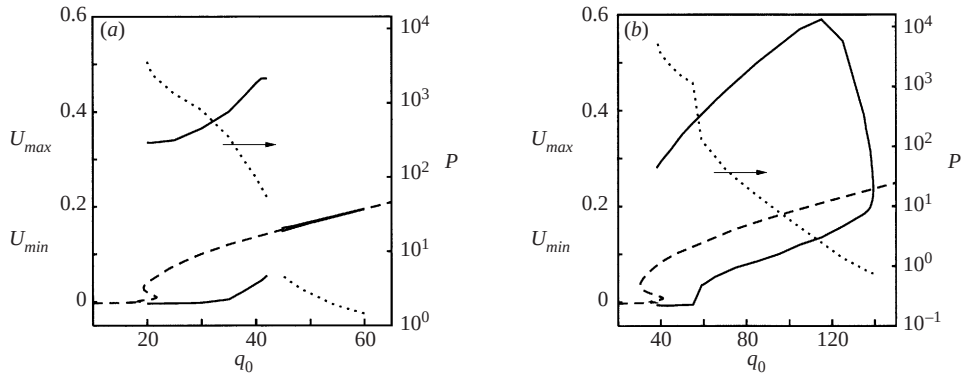

FIGURE 8. Minimum and maximum spread rate in the pulsating regime (solid), spread rate of the unstable stationary solution (dashed), and period of the oscillation (dotted, right-hand ordinate), as functions of q_0 for $Re = 1000$, $Pr = 10$ and the two values $\lambda = 0.2$ (*a*) and $\lambda = 0.02$ (*b*).

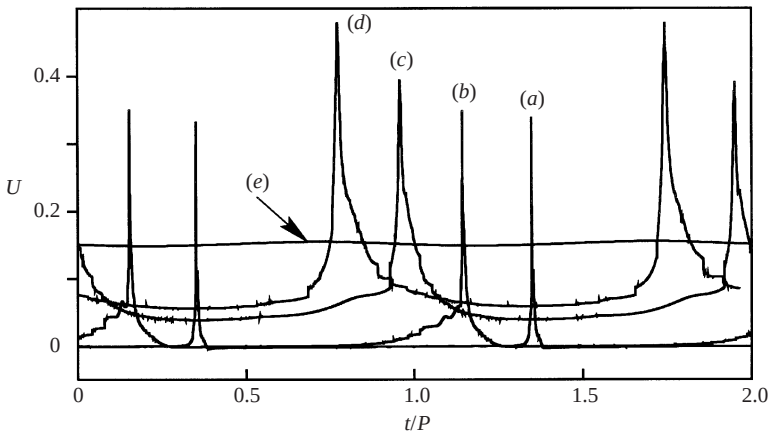

FIGURE 9. Instantaneous spread rate during two cycles of the oscillation for $Re = 1000$, $Pr = 10$, $\lambda = 0.2$ and $q_0 = 20$ (*a*), 30 (*b*), 40 (*c*), 42 (*d*), and 45 (*e*). The time is scaled with the period of the oscillations to make the curves comparable.

instantaneous spread rate is given in figure 9 as a function of time (scaled with the period) for two cycles of the oscillation and different values of q_0. All these results are in qualitative agreement with experiments (Akita & Fujiwara 1971; Akita 1973; Ito *et al.* 1991; García-Ybarra *et al.* 1994).

Figure 8(*a*) shows that there are apparently two types of oscillation for $\lambda = 0.2$. A branch of oscillatory solutions bifurcates from the stationary solution at a relatively large value of q_0 for which the stationary solution has no recirculation region. The amplitude of these oscillations remains small in a range of q_0 extending from their inception to a value slightly below that for which recirculation first appears in the stationary solution, and then, suddenly, the oscillations switch to a large-amplitude, low-frequency mode. The connection between the two modes is not clear. Numerical computations show that the solution is not periodic in a narrow transition range of q_0, and no hysteresis was detected. The two oscillatory modes could be parts of a unique branch, which for some reason has a very slender S shape, or they could belong to different branches separated by more complex solutions, such as a sequence of period doubling, a window of chaos, and intermittency. The numerical method used

here is not sufficiently accurate, and each individual computation is too expensive numerically, to try to settle this issue.

The oscillations of the second branch (left-hand side of figure 8*a*) are finite-amplitude, non-sinusoidal oscillations from the beginning. They become relaxation oscillations when q_0 decreases, featuring long intervals of small, even negative spread rate and short pulses of fast spread. These are the crawling and jump phases observed experimentally. The period of the oscillations and the sharpness of the spikes increase with decreasing q_0, until the oscillations disappear at a value of q_0 that apparently coincides with the lowest turning of the stationary response curve. This fact and the similarity between the flow pattern in the intervals of slow spread and the stationary solution, to be discussed below, supports the hypothesis of a saddle–node infinite-period bifurcation at the low-q_0 end of the pulsating regime (García-Ybarra *et al.* 1994).

A single branch of oscillatory solutions exists for $\lambda = 0.02$ (figure 8*b*). This branch bifurcates from the stationary solution at a value of q_0 for which there is already recirculation, increases rapidly in amplitude with decreasing q_0, and becomes qualitatively similar to the second oscillatory branch of the previous case. In the range $58 > q_0 > 56$, the train of spikes, which by then are clearly identifiable, splits into groups spaced by increasing intervals of small spread rate. This leads to a rapid increase of the overall period. At $q_0 = 55$ the jump phases of the oscillation consist of pairs of spikes, which become trios when q_0 decreases below about 40.

Further details of each oscillatory mode are discussed separately in the rest of this section.

5.1. *Relaxation oscillations*

Consider first the large-amplitude relaxation oscillations that occur for small values of q_0, which are the type of oscillation most clearly observed experimentally. Figure 10 shows the temperature field for $Re = 5000$, $Pr = 10$, $q_0 = 80$ and $\lambda = 0.2$ at six instants during a cycle, marked on the spread rate curve in figure 11. This value of q_0 is rather to the left on the branch of oscillatory solutions, but most of the description that follows applies to the whole branch and also to values of λ smaller than 0.2. Figure 10 is to be compared with other numerical computations (Di Blasi *et al.* 1990, 1991; Schiller *et al.* 1996) and flow visualizations (Ito *et al.* 1991; Ross 1994 and references therein).

Figure 10(*a*) is for a time shortly after a peak of the spread rate. Most of the liquid is cool and the momentum flux injected into the liquid by the thermocapillary stresses concentrated immediately to the left of the origin has created an eddy that moves toward the left under the induction of its image above the surface. The warm liquid in the upper part of the eddy originates a tongue that projects toward the left, driven by local thermocapillary stresses. The eddy and its tongue grow for some time after the beginning of the crawling phase (figure 10*b*). Apparently, the growth of the tongue is enhanced by the presence of the eddy, which creates a region of low velocity on its upstream side. The temperature of the tongue and the upper part of the eddy is high at the beginning and decreases as both elements grow and move away from the origin.

The growth slows down and comes to an end when the bottom of the layer begins to affect the eddy. Then the eddy becomes elongated and begins to shed slightly warm liquid from its lower-left side (figure 10*c*). For some time the right-bound motion of this liquid coexists with the left-bound motion of the upper-left part of the eddy and

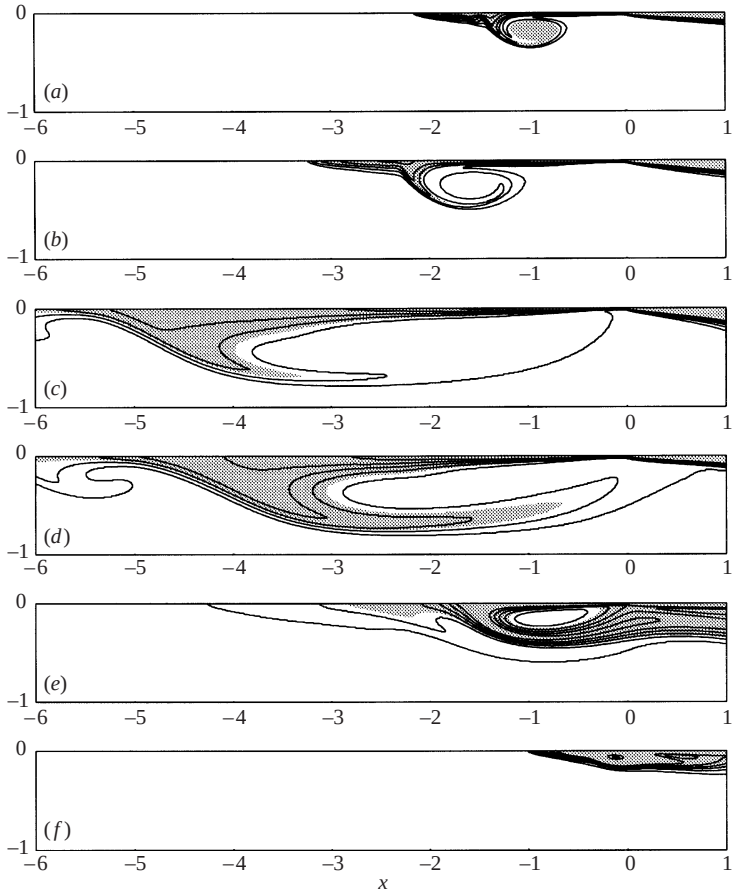

FIGURE 10. Six snapshots of the temperature field during a cycle of the relaxation oscillation for $Re = 5000$, $Pr = 10$, $\lambda = 0.2$ and $q_0 = 80$. See figure 11 for the description of (*a*)–(*f*).

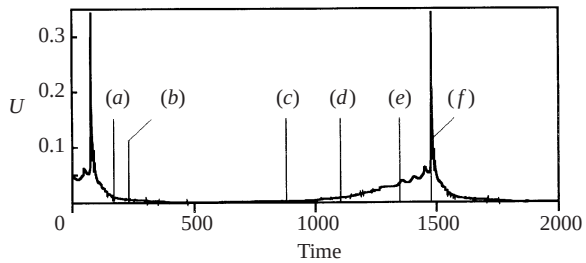

FIGURE 11. Spread rate as a function of time for the case of figure 10.

its tongue. This process is very slow and very little change is observed in the bulk of the eddy, whose shape resembles the stationary solutions of § 3.

When the slightly warm liquid from the lower side of the eddy reaches the vicinity of the origin (figure 10*d*) it elicits only a weak response of the region around the origin controlling the spread rate (cf. § 4.3), because the temperature of the returning liquid is so low that it makes little difference to the case when the controlling region feeds on cool liquid from everywhere but its right-hand side. The overall picture is

still close to a stationary flow. Very slowly, however, the liquid approaching the origin from the bottom of the eddy becomes a little warmer and the controlling region responds by increasing slightly the spread rate. This increase has a noticeable effect on the bulk of the eddy and its tongue, because the velocity of the liquid is very small in these regions. The eddy shortens and the liquid recirculating in its lower part becomes warmer because it has less time to lose its heat to the cool core of the eddy above it or to the liquid flowing underneath (compare figures 10*c*, 10*d* and 10*e*). When the warm liquid approaches the origin, the controlling region adjusts by further increasing the spread rate, in such a way that a fraction of this liquid reaches the surface only past the origin, without affecting the controlling region, which is partially bathed by the cool liquid forming the core of the eddy.

The length and depth of the eddy decrease steadily, leaving a fast cool stream in the lower part of the layer, and the tongue nearly collapses on to the left-hand side of the eddy (figure 10*e*). However, the surface jet to the left of the origin keeps active and pumping liquid toward the left, which creates a parcel of low velocity under the jet hosting the cool shrinking core of the eddy and preventing its being swept away along with the warm liquid at deeper strata (figure 10*e*). As the spread rate increases the size of the cool core decreases and it moves closer to the origin, but it continues to block the access to the controlling region of most of the warm liquid that flows underneath.

Finally, when the core is almost depleted, the jet sucks warm liquid from the right into the controlling region, decreasing the value of $\mathrm{d}\theta/\mathrm{d}\psi$ in the liquid that enters this region and making it impossible to fulfil the equilibrium condition discussed in § 4.3. It is in this last stage of the cycle that propagation switches to the fast solid-like mode of § 3 and the remnants of the cool core are washed out (figure 10*f*). The fast propagation phase lasts only while the preheated liquid at the left of the origin, which by now occupies only a short length, flows under the origin, and it ends abruptly when the front enters the cool incoming stream. The surface temperature gradient is then at its highest, the concentrated thermocapillary force leads to a new tiny eddy, and the process repeats.

The above description is essentially valid for larger q_0 on the branch of oscillatory solutions. The main change observed when q_0 increases is that the eddy that appears at the beginning of the crawling phase may never reach the bottom of the layer, its growth being arrested by the incoming stream, which is strong at any moment of the cycle when q_0 is large. Other differences are that the disparity of time scales between the jump and crawling phases is reduced, and that the small cool core of the eddy does not stop at the origin at the beginning of the jump phase. This core is seen downstream of the origin, being washed out, during part of the jump phase.

On the other hand, when q_0 decreases toward the left end of the oscillatory branch, the duration of the crawling phase increases and the flow in this phase resembles more and more the stationary solutions of figure 1. It seems that, eventually, the eddy becomes so long and the recirculating liquid loses so much heat to the bottom before reaching the origin that it cannot trigger an increase of the spread rate, and therefore the crawling phase lasts forever, giving way to the pseudo-uniform regime.

5.2. *Small-amplitude oscillations*

The small-amplitude oscillations appear before the stationary flow develops recirculation, and they can be understood in terms of a delay between the formation of temperature perturbations about the stationary temperature and the influence of these perturbations on the spread rate. A condition for the delay to develop is the existence

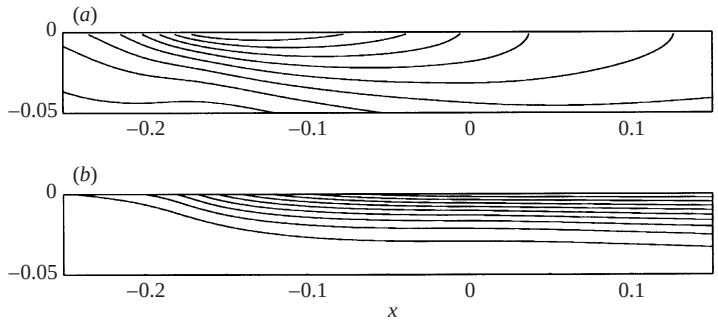

FIGURE 12. (*a*) Time-averaged horizontal velocity (nine contours between $u = 0$ and $u = 0.16$) and (*b*) temperature (eleven contours between $\theta = 0$ and $\theta = 1$) in the upper twentieth of the liquid layer for $Re = 1000$, $Pr = 10$, $\lambda = 0.2$ and $q_0 = 55$.

of a sufficiently long region of low velocity by the surface ahead of the vaporization front, which happens when the width λ of the surface heat flux distribution is large (cf. figure 2).

Figure 12 shows the average temperature and horizontal velocity for a point on the branch of small-amplitude oscillations. These fields have been obtained by averaging the instantaneous variables over a large number of cycles and are virtually indistinguishable from the stationary solution for the same values of the parameters. The spread rate (not shown) oscillates sinusoidally with an amplitude of about one hundredth of its stationary value. As can be seen, both the surface temperature and the temperature in a layer around the surface increase monotonically with the streamwise distance. The horizontal velocity has a minimum at the surface some distance upstream of the origin, where recirculation will first appear when q_0 is decreased.

The temperature perturbation in the upper twentieth of the layer, obtained by subtracting the average temperature from the instantaneous temperature, is given in figure 13 at six different times spanning half an oscillation cycle. The horizontal bar above each temperature field represents the instantaneous spread rate perturbation about its stationary value, which is the vertical tic in the middle.

The liquid always approaches the origin from the left in the absence of reverse flow, and the region around the origin enforcing the regularity condition $A = 0$ of § 2 responds qualitatively the same as for a solid fuel. When this region is surrounded by a positive temperature perturbation, the spread rate increases in order to offset the perturbation with an excess of cool liquid from the base flow ahead of the origin and satisfy the condition of regularity. Similarly, the spread rate decreases when a portion of liquid with a temperature defect surrounds the origin.

Temperature perturbations are generated in the present oscillatory regime because the liquid passes under the time-independent surface heat flux distribution with varying velocity. Thus a temperature defect exists on the left-hand side of the surface in figure 13*a* because the spread rate has been high for some time and the surface heat flux has not been able to heat the liquid as much as it would do in the stationary regime. For the same reason, the temperature excess in the central part of this figure, which was formed at an early time when the spread rate was low, is now sinking into the liquid. This central portion of high temperature is in fact responsible for the present high spread rate, which remains above its mean value until about figure 13(*c*), when the temperature defect formerly at the left begins to affect the origin. Then the

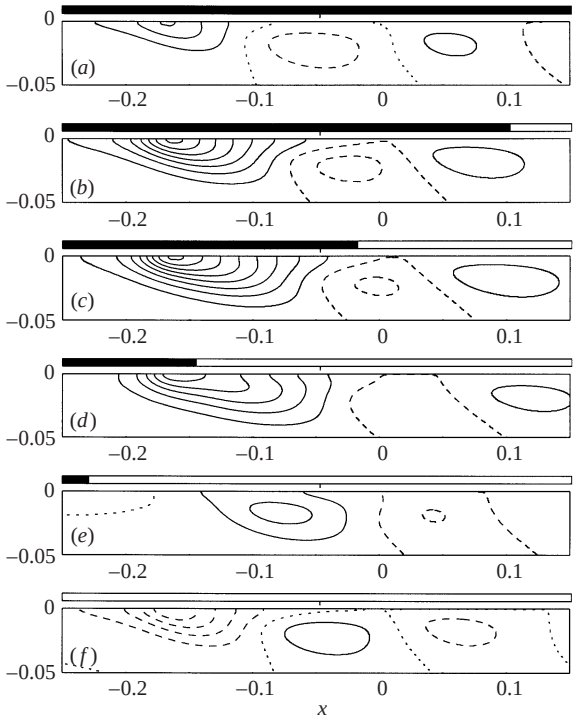

FIGURE 13. Six snapshots of the temperature perturbation during half a cycle of the small-amplitude oscillation for $Re = 1000$, $Pr = 10$, $\lambda = 10$ and $q_0 = 55$. Solid contours are temperature defects, between -1.6×10^{-3} and 0, and dashed contours are temperature excesses, between 0 and 10^{-3}. The lengths of the upper bars are proportional to the instantaneous spread rate perturbation.

spread rate decreases (figure 13*d*) and the excess of heat received by the slow moving liquid begins to build up a new temperature excess (left hand sides of figures 13*e* and 13*f*) and to confine the temperature defect to the interior of the liquid. The influence of the temperature defect on the spread rate is nearly at its maximum in the last figure of the sequence, which is similar to the first figure but with the positions of the temperature excesses and defects exchanged. The evolution during the second half of the cycle is the image of that shown for the first half.

The elements of the above description are common to flame spread over liquid fuels without recirculation, which is oscillatory, and to flame spread over solid fuels, which is not. The key difference seems to be the non-uniform base velocity of the liquid (figure 12*a*). As can be seen in the sequence of figure 13, the temperature defect originating at the left-hand side does not move uniformly in the streamwise direction; instead, it stays anchored for some time to the minimum of the velocity and then shoots to the origin. This generates a deep localized temperature defect that reaches the origin and affects the spread rate before suffering much diffusion to its surroundings. Thus, while the cause of the temperature perturbations is the time variation of the spread rate, the perturbations themselves are convected mainly by the base flow. Convection of the temperature perturbations by the velocity perturbations would be a second-order effect in a linear stability analysis and seems to be negligible here because the perturbations are small.

In order to check this hypothesis, a model problem was considered in which the energy equation (2.3) was solved with a velocity field equal to the stationary,

time-averaged velocity plus a time-dependent uniform component whose strength is chosen to satisfy the regularity condition at the origin. This leaves out the velocity perturbation induced by the perturbation of the thermocapillary stress. The model still shows oscillations, which are in fact of growing amplitude. As a second test, only the uniform velocity component was left in (2.3), which then mimics the situation with a solid fuel. The oscillations disappear in this case.

5.3. *Comparisons with experiments*

It was mentioned below (2.9) that there is a correspondence between increasing q_0 and increasing the initial temperature of the liquid T_0. This correspondence, however, is not an exact one because T_0 appears not only in the non-dimensionalization of q_0 but also in the definition of the Reynolds number in (2.8) and in other non-dimensionalization factors. Strictly, q_0 reflects the exothermicity of the gas-phase reactions and should increase with the oxygen concentration of the gas. Seen in this light, the results of figure 8 are in qualitative agreement with the experimental results of Miller *et al.* (2000) for different oxygen concentrations.

Regarding the dependence of the results on the initial temperature of the liquid T_0, it is well-known experimentally that a transition from pulsating spread to uniform spread occurs as T_0 is increased, and that, within the pulsating regime, the period and the amplitude of the pulsation decrease as T_0 increases. To check these trends beyond the approximation implicit in the correspondence between q_0 and T_0, additional computations have been carried out in which the variation of Re and all the non-dimensionalization factors with T_0 is taken into account. To this end, the results for $Re = 1000$, $Pr = 10$, $q_0 = 125$ and $\lambda = 0.02$, which is a case in the pulsating regime in figure 8(b), are taken as a base (denoted with a superscript $*$ in what follows). If this base case is assumed to correspond to a certain $T_0 = T_0^*$, and T_0 is changed keeping all the other physical parameters constant, then the non-dimensional value of q_0 will become $q_0 = q_0^*\xi$, with $\xi = (T_v - T_0^*)/(T_v - T_0)$, while $Re = Re^*/\xi$ and the values of the non-dimensional spread rate and the non-dimensional period of the pulsation are to be multiplied by ξ^{-1} and ξ, respectively, so that they are scaled with the constant values $v_c^* = |\sigma'|(T_v - T_0^*)/\mu$ and h/v_c^* when T_0 varies. The results obtained by increasing ξ above 1, which amounts to increasing T_0 above T_0^*, are shown in figure 14(a). These results conform qualitatively to the experimental results mentioned above. The increase of the spread rate with T_0 is dwarfed in figure 14(a) by the large values of the peak spread rate in the pulsating regime, which are larger than observed experimentally, though they are attained only during very short periods of time (see figures 9 and 11).

The dependence of the pulsation period and amplitude on the pool depth h at a given initial temperature has been also investigated experimentally, and both magnitudes have been found to increase with h. To compare with these experimental results, it must be noticed that when h is multiplied by a factor ζ leaving all the other physical parameters constant, (Re, q_0, λ) are multiplied by (ζ, ζ, ζ^{-1}), respectively, while the non-dimensional time is to be multiplied by ζ and the scale of the velocity is not altered. The spread rates during about two pulsation cycles are plotted in figure 14(b) for the base case $(Re, q_0, \lambda) = (520, 65, 0.0385)$ and the case $(Re, q_0, \lambda) = (760, 95, 0.0263)$, which is obtained from the base case with $\zeta = 1.462$ and thus corresponds to a deeper pool. The results are in qualitative agreement with the experiments.

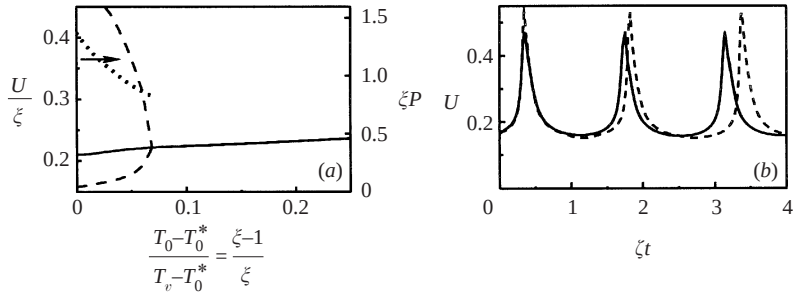

FIGURE 14. (*a*) Spread rate as a function of the initial temperature of the liquid. The average spread rate (solid), minimum and maximum spread rates (dashed), and period (dotted) are shown for the pulsating regime at the left of the figure. (*b*) Instantaneous spread rate as a function of time for the two cases $(Re, q_0, \lambda) = (520, 65, 0.0385)$ (solid) and $(Re, q_0, \lambda) = (760, 95, 0.0263)$ (dashed). $Pr = 10$ in all the cases.

6. Conclusions

The thermocapillary flow induced in a liquid layer by a surface heat flux distribution that mimics the effect of a flame spreading over the liquid surface has been studied numerically and asymptotically. The spread rate is determined, in this model, by a condition of regularity at the vaporization front where the surface temperature first reaches the vaporization temperature of the liquid.

The stationary rate of spread (U) has been computed as a function of the strength of the surface heat flux distribution (q_0) for different values of the width of this distribution and of a Reynolds number based on the thermocapillary velocity. The stationary solution shows a quadratic dependence of U on q_0 for large values of this parameter, a critical q_0 below which recirculation appears, and a region of multiplicity, with three different branches of $U(q_0)$, when the Reynolds number is sufficiently high. The spread rate vanishes for a certain positive q_0 within a second small region of multiplicity, and then becomes negative and decreases rapidly with decreasing q_0.

An asymptotic analysis of the low-spread-rate stationary solutions has been carried out for large Reynolds numbers, for which the flow features a long recirculation bubble extending far ahead of the vaporization front. Special attention has been given to a small region around the vaporization front which plays a key role in determining the spread rate in the presence of recirculation. This region imposes a relationship between q_0 and the temperature gradient in the liquid that enters this region from behind. The temperature gradient, on the other hand, depends on the flow in the rear part of the recirculation bubble, under the vaporizing surface, where there is a thermal surface layer whose extent, and thus the value of the temperature gradient, depends on the spread rate. In these conditions, giving the temperature gradient as a function of q_0 amounts to giving $U(q_0)$.

A description of the relaxation oscillations in the pulsating regime has been proposed on the basis of the numerical results. According to this description, the small region around the vaporization front controls the spread rate during most of the oscillation cycle, and it triggers pulses of fast spread in conjunction with the delay and feedback created by the recirculating flow. An eddy and a surface layer of warm liquid move and grow ahead of the vaporization front during the crawling phase of small spread rate, the eddy being propelled by its image above the surface and both elements growing under the continuous supply of momentum and warm liquid provided by a thermocapillary force concentrated immediately to the left of the

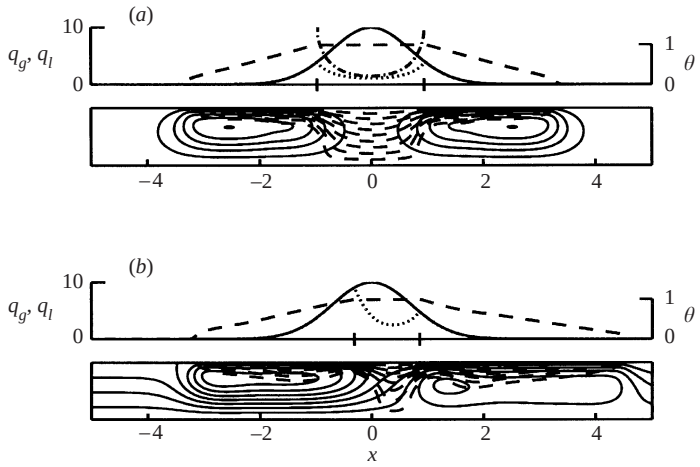

FIGURE 15. Flow induced by a Gaussian heat source for $Ma = Re\,Pr = 10^4$, $Re = 0$, $q_0 = 10$, $\lambda = 1$ and the two values $U = 0$ (a) and $U = 0.02$ (b). The streamlines (solid) and isotherms (dashed) of the flow are displayed in the lower part of each figure, while the upper parts show the distributions of q_g (solid), surface temperature (dashed), and the heat flux entering the liquid (dotted). The vaporizing region extends between the two vertical tics. The dash-and-dot curve in the upper figure illustrates the divergence of q_l at the boundaries of the vaporization region when their positions are assigned arbitrarily.

vaporization front. Most of the liquid that enters the controlling region in this phase is cool, and the spread rate adjusts to a small value in order for this region to entrain the correct amount of warm liquid from under the vaporizing surface. After some time, however, the incoming stream or the bottom of the channel arrest the growth of the eddy and some slightly warm recirculating liquid approaches the controlling region and leads to a self-accelerating increase of the spread rate that marks the end of the crawling phase and forces the transition to the jump phase, during which the vaporization front advances over the remnants of the region preheated by the eddy.

I am indebted to P. L. García-Ybarra for useful discussions. This work was supported by DGES grant PB98-0142-C04-04.

Appendix. Gaussian heat source

Let a heat source move with a given velocity U above the surface of a liquid layer. The source yields a Gaussian distribution of heat flux to the surface, heating the liquid and inducing a thermocapillary flow in it. The maximum temperature of the surface should increase when the strength of the source increases or its velocity decreases, until, for sufficiently high values of the strength and sufficiently low velocities, the liquid will vaporize in a certain region of the surface that moves with the source. The flow and the temperature distribution in a reference frame moving with the source satisfy (2.1)–(2.3) with the boundary conditions (2.4a, b), (2.5), and (2.6), which also applies for $x \to \infty$. If x_1 and x_2 are the positions of the leading and trailing boundaries of the vaporization region, which are to be determined as part of the solution, condition (2.4c) becomes

$$\frac{\partial \theta}{\partial y} = q_g(x) \text{ for } x < x_1 \text{ and } x > x_2 \quad \text{and} \quad \theta = 1 \text{ for } x_1 < x < x_2, \tag{A 1}$$

with $q_g(x)$ given by (2.9) for any x.

Only the distribution of $q_g(x)$ outside the vaporization region appears in this formulation. The heat flux that enters the liquid in the vaporizing region $x_1 \leqslant x \leqslant x_2$, i.e. $q_l = \partial\theta/\partial y|_{y=0}$, should be determined by the solution of the problem. The difference $q_g(x) - q_l(x)$ is the heat flux used to vaporize the liquid.

If x_1 and x_2 are assigned arbitrary values, then the square-root behaviour of the temperature discussed in § 2 will appear around these points, leading to $\theta - 1 = A_1 r_1^{1/2} \sin\varphi_1/2$ for $r_1 \ll 1$ and $\theta - 1 = A_2 r_2^{1/2} \sin\varphi_2/2$ for $r_2 \ll 1$, where r_1 and r_2 are the distances to the leading and trailing boundaries of the vaporization region, φ_1 and φ_2 are the angles around these points, and A_1 and A_2 are constants that depend on the parameters of the problem (U, Re, Pr, q_0, λ), and on x_1 and x_2. This gives $q_l \sim A_1/2(x - x_1)^{1/2}$ when $x \searrow x_1$ and $q_l \sim A_2/2(x_2 - x)^{1/2}$ when $x \nearrow x_2$, which is not admissible because q_l cannot be larger than q_g. Therefore the two conditions $A_1 = A_2 = 0$ must be imposed, determining the unknowns x_1 and x_2.

Two sample numerical solutions of the problem are displayed in figure 15 for $Ma = Re\,Pr = 10^4$, $Re = 0$ (creeping flow), $q_0 = 10$, $\lambda = 1$, and the two values $U = 0$ and $U = 0.02$. The lower part of each panel shows the streamlines and isotherms, which are symmetric about $x = 0$ when $U = 0$. The upper parts show the heat flux reaching the surface (q_g, solid), the heat flux entering the liquid (q_l, dotted), and the surface temperature (dashed). The dash-and-dot curve of figure 15*a* illustrates the diverging q_l that is obtained when λ is changed to 0.5 keeping x_1 and x_2 fixed.

REFERENCES

Akita, K. 1973 Some problems of flame spread along a liquid surface. *Proc. Combust. Inst.* **14**, 1075–1083.

Akita, K. & Fujiwara, O. 1971 Pulsating flame spread along the surface of liquid fuels. *Combust. Flame* **17**, 268–269.

Buckmaster, J., Hegab, A. & Jackson, T. L. 2000 More results on oscillating edge-flames. *Phys. Fluids* **12**, 1592–1600.

Buckmaster, J. & Zhang, Yi. 1999 Oscillating edge-flames. *Combust. Theory Modelling* **3**, 547–565.

Degroote, E. & García-Ybarra, P. L. 2000 Flame spreading over liquid ethanol. *Eur. Phys. J.* B **13**, 381–386.

Degroote, E. & García-Ybarra, P. L. 2002 Steady propagation regimes for flame spread over liquid alcohols. *Phys. Fluids*, submitted.

Di Blasi, C., Crescitelli, S. & Russo, G. 1990 Model of pulsating flame spread across liquid fuels. *Proc. Combust. Inst.* **23**, 1669–1675.

Di Blasi, C., Crescitelli, S. & Russo, G. 1991 Model of oscillatory phenomena of flame spread along the surface of liquid fuels. *Comput. Meth. Appl. Mech. Engng.* **90**, 643–657.

Fernández-Pello, A. C., Kindelán, M. & Williams, F. A. 1974 Distribución superficial de temperaturas durante la propagación de llamas en sentido descendente sobre láminas de PMMA. *Ing. Aeron. Astron.* **133**, 41–53.

Furuta, M., Humphrey, J. A. C. & Fernández-Pello, A. C. 1985 Prediction of flame spread hydrodynamics over liquid fuel. *PhysicoChem. Hydrodyn.* **6**, 347–372.

Garcia-Ybarra, P. L., Antoranz, J. C., Sankovitch, V. & Castillo, J. L. 1994 Experimental evidence of self-excited relaxation oscillations leading to homoclinic behavior in spreading flames. *Phys. Rev.* E **49**, 5225–5229.

Garcia-Ybarra, P. L., Castillo, J. L., Antoranz, J. C., Sankovitch, V. & San Martin J. 1996 Study of the thermocapillary layer preceding slow, steadily spreading flames over liquid fuels. *Proc. Combust. Inst.* **26**, 1469–1475.

Glassman, I. & Dryer, F. L. 1981 Flame spread across liquid fuels. *Fire Safety J.* **3**, 123–138.

Higuera, F. J. 1999 Downward flame spread along a vertical surface of a thick solid in the thermal regime. *Combust. Theory Modelling* **3**, 147–158.

HIGUERA, F. J. 2000 Steady thermocapillary-buoyant flow in an unbounded liquid layer heated nonuniformly from above. *Phys. Fluids* **12**, 2186–2197.

HIGUERA, F. J. & GARCÍA-YBARRA, P. L. 1998 Steady and oscillatory flame spread over liquid fuels. *Combust. Theory Modelling* **2**, 43–56.

HIRANO, T., SUZUKI, T., MASHIKO, I. & TANABE, N. 1980 Gas movements in front of flames propagating across methanol. *Combust. Sci. Technol.* **22**, 83–91.

ITO, A., MASUDA, D. & SAITO, K. 1991 A study of flame spread over alcohols using holographic interferometry. *Combust. Flame* **83**, 375–389.

KIM, I., SCHILLER, D. N. & SIRIGNANO, W. A. 1999 Axisymmetric flame spread across propanol pools in normal and zero gravities. *Combust. Sci. Technol.* **139**, 249–275.

KONISHI, T., TASHTOUSH, G., ITO, A., NARUMI, A. & SAITO, K. 2000 The effect of a cold temperature valley on pulsating flame spread over propanol. *Proc. Combust. Inst.* **28**, 2819–2826.

LIÑÁN, A. 1985 Theory of droplet vaporization and combustion. In *Modélisation des Phénomènes de Combustion* (ed. R. Borghi, P. Clavin, A. Liñán, P. Pelcé & G. I. Sivashinsky), pp. 73–103. Eyrolles.

LIÑÁN, A. 1994 Ignition and flame spread in laminar mixing layers. In *Combustion in High Speed Flows* (ed. T. L. Jackson, J. Buckmaster & R. Kumar), pp. 461–476. Kluwer.

MACKINVER, R., HANSEL, J. G. & GLASSMAN, I. 1968 Influence of laboratory parameters on flame spread across liquid fuels. *Combust. Sci. Technol.* **1**, 293–306.

MILLER, F. J. & ROSS, H. D. 1992 Further observations of flame spread over laboratory-scale alcohol pools. *Proc. Combust. Inst.* **24**, 1703–1711.

MILLER, F. J. & ROSS, H. D. 1995 Liquid-phase velocity and temperature fields during uniform flame spread over 1-propanol. *Proc. Intl Symp. on Transport Processes.*

MILLER, F. J. & ROSS, H. D. 1998 Smoke visualization of the gas-phase flow during flame spread across a liquid pool. *Proc. Combust. Inst.* **27**, 2715–2722.

MILLER, F. J., ROSS, H. D., KIM, I. & SIRIGNANO, W. A. 2000 Parametric investigation of pulsating flame spread across 1-butanol pools. *Proc. Combust. Inst.* **28**, 2827–2833.

ROSS, H. D. 1994 Ignition of and flame spread over laboratory-scale pools of pure liquid fuels. *Prog. Energy Combust. Sci.* **20**, 17–63.

ROSS, H. D. & MILLER, F. J. 1997 Gravitational and low-speed convective effects on flame spread across liquid fuel pools: A comparative analysis. *5th Intl Symp. Fire Safety Sci.* (ed. Y. Hasemi). Interscience Communications Ltd; to be submitted to *Fire Safety J.*

SCHILLER, D. N., ROSS, H. D. & SIRIGNANO, W. A. 1996 Computational analysis of flame spread across alcohol pools. *Combust. Sci. Technol.* **118**, 203–258.

SCHILLER, D. N. & SIRIGNANO, W. A. 1997 Opposed-flow flame spread across n-propanol pools. *Proc. Combust. Inst.* **26**, 1319–1325.

SHARMA, O. P. & SIRIGNANO, W. A. 1971 A hydrodynamical analysis of the flame spreading over liquid fuels. *AIAA Paper* 71–207.

SIRIGNANO, W. A. & GLASSMAN, I. 1970 Flame spreading above liquid fuels: surface-tension-driven flows. *Combust. Sci. Technol.* **1**, 307–312.

TORRANCE, K. E. 1971 Subsurface flows preceding flame spread over a liquid fuel. *Combust. Sci. Technol.* **3**, 133–143.

TORRANCE, K. E. & MAHAJAN, R. L. 1975*a* Surface tension flows induced by a moving thermal source. *Combust. Sci. Technol.* **10**, 125–136.

TORRANCE, K. E. & MAHAJAN, R. L. 1975*b* Fire spread over liquid fuels: liquid phase parameters. *Proc. Combust. Inst.* **15**, 281–287.

WICHMAN, I. S. 1992 Theory of opposed-flow flame spread. *Prog. Energy Combust. Sci.* **18**, 553–593.

WICHMAN, I. S. & WILLIAMS, F. A. 1983 A simplified model of flame spread in an opposed flow along a flat surface of a semi-infinite solid. *Combust. Sci. Technol.* **32**, 91–123.

WILLIAMS, F. A. 1985 *Combustion Theory*, Chap. 9, 2nd edn. Benjamin-Cummings.